Advances in Differential Equations and Control Processes 2026, 33(3), 4725.
doi: https://doi.org/10.59400/adecp4725

Article

Dynamical behavior of an HIV infection model with treatment failure, adherence, and drug resistance

Maria Batool[1], Israr Ali Khan[1,*], Rashid Jan[2], Muhammad Shoaib Arif[3], Ateeq Ur Rehman[3]

[1] Institute of Numerical Sciences, Kohat University of Science and Technology, Kohat 26000, Pakistan; mahemalik56@gmail.com
[2] Department of Mathematics, College of Science, Qassim University, Buraydah 51452, Saudi Arabia; r.jehan@qu.edu.sa
[3] Department of Mathematics and Sciences, College of Sciences and Humanities, Prince Sultan University, Riyadh 11586, Saudi Arabia; marif@psu.edu.sa (MSA); airshad@psu.edu.sa (AUR)
*** Corresponding author:** Israr Ali Khan, israrali@kust.edu.pk

CITATION

Batool M, Khan IA, Jan R, et al. Dynamical behavior of an HIV infection model with treatment failure, adherence, and drug resistance. Advances in Differential Equations and Control Processes. 2026; 33(3): 4725. https://doi.org/10.59400/adecp4725

ARTICLE INFO

Received: 26 July 2026
Revised: 15 August 2026
Accepted: 20 August 2026
Available online: 4 September 2026

Abstract: Imperfect adherence to antiretroviral therapy (ART), virological failure, and the emergence of drug-resistant human immunodeficiency virus (HIV) strains continue to limit the long-term effectiveness of HIV control programmes. Existing deterministic models generally treat these mechanisms separately, so the pathway linking imperfect adherence to acquired resistance is seldom represented explicitly. We formulate a seven-compartment HIV transmission model in which stage-structured progression, ART initiation, adherence-mediated treatment failure, and acquired drug resistance appear as sequential, mechanistically linked transitions within a single tractable system. The model is shown to be well-posed: solutions remain non-negative and bounded, and a biologically feasible region is positively invariant. The basic reproduction number $\mathscr{R}_0$ is obtained in closed form by the next-generation matrix method and separates into progression-driven and acquired immunodeficiency syndrome (AIDS)-mediated contributions, which makes the weight of each transmission pathway explicit. The disease-free equilibrium is locally and globally asymptotically stable when $\mathscr{R}_0 < 1$, whereas a unique endemic equilibrium exists whenever $\mathscr{R}_0 > 1$. Local asymptotic stability of the endemic equilibrium is conditional on the associated Routh–Hurwitz criteria and is verified numerically for the baseline parameter set through direct computation of the Jacobian eigenvalues. Normalised sensitivity indices rank the transmission rate first, followed by parameters governing the treatment-failure and drug-resistant compartments. An optimal control problem combining prevention, treatment uptake, and adherence support is characterised through Pontryagin's Maximum Principle and solved by a forward–backward sweep; the combined strategy lowers the infected burden relative to the uncontrolled case over the horizon considered.

Keywords: HIV dynamics; nonlinear systems; antiretroviral therapy adherence; treatment failure; acquired drug resistance; stability analysis; optimal control

1. Introduction

Human immunodeficiency virus (HIV) infection remains one of the most significant global public-health challenges of the modern era. Despite remarkable advances in HIV prevention, diagnosis, and treatment, the disease continues to pose a substantial epidemiological and socioeconomic burden worldwide. According to recent estimates reported by the Joint United Nations Programme on HIV/AIDS (UNAIDS), approximately 40.8 million people were living with HIV in 2024, with

1.3 million new HIV infections and approximately 630,000 AIDS-related deaths recorded globally [1, 2]. The widespread use of antiretroviral therapy (ART) has substantially reduced HIV-related mortality, improved life expectancy among people living with HIV, and transformed HIV infection from a fatal disease into a manageable chronic condition [3]. Nevertheless, the long-term effectiveness of ART-based control strategies is increasingly threatened by suboptimal treatment adherence, treatment failure, and the emergence of drug-resistant HIV strains. HIV transmission dynamics are inherently nonlinear and involve multiple biological and epidemiological stages [4]. Following infection, individuals typically progress through the acute, chronic, and AIDS stages of the disease, each characterized by distinct levels of viral activity, infectiousness, and immune response [5, 6]. Since transmission potential varies considerably across these stages, incorporating such heterogeneity is essential for accurately describing HIV transmission dynamics. Although ART substantially reduces viral load and the risk of onward transmission, its effectiveness depends critically on sustained adherence to the prescribed treatment regimen. Poor adherence can compromise treatment success, promote virological failure, and facilitate the emergence of drug-resistant HIV strains [7, 8].

Mathematical modelling has become an indispensable tool for understanding the dynamics of infectious diseases and evaluating intervention strategies. The compartmental epidemic models introduced by Anderson and May [9] and subsequently refined by Hethcote [10] provide the foundation for modern mathematical models of HIV transmission. Over the past several decades, numerous mathematical models have been developed to investigate HIV transmission, treatment dynamics, behavioural interventions, and the emergence of drug resistance [7,8]. Fractional-order formulations have also been employed to incorporate memory effects and nonlocal dynamics into epidemiological systems [11]. In the context of HIV modelling, Kongson et al. [12] investigated a fractal-fractional HIV infection model in the Atangana–Baleanu sense to evaluate the effects of drug therapy, while Khan et al. [13] formulated a fractional-order HIV–TB coinfection model with a nonsingular Mittag–Leffler kernel. Related fractional modelling based on a power-law-type kernel has also been applied to co-abuse dynamics [14]. In addition, delay-differential formulations have been used to account for the time lags inherent in disease progression and treatment response [15]. Liu et al. [16] studied global stability in a within-host HIV pathogenesis model with a cure rate, whereas Huo and Feng [17] examined an HIV/AIDS epidemic model with different latent stages and treatment. Recent work has also developed optimal-control and fractional-order HIV frameworks with stage structure and treatment dynamics [18, 19], as well as stochastic, syndemic, and data-driven extensions [20–22]. Although these models have provided valuable insights into HIV transmission and disease progression, most existing studies investigate treatment adherence, treatment failure, and drug resistance separately, rather than integrating these mechanisms within a unified epidemiological framework. From the perspective of mathematical epidemiology, one of the central objectives is to characterize the threshold dynamics of disease transmission through the basic reproduction number, $\mathscr{R}_0$. Among the available analytical techniques, the next-generation matrix approach developed by Diekmann et al. [23] and van den Driessche and Watmough [24] remains one of the most widely used methods for deriving $\mathscr{R}_0$ and investigating disease persistence. Stability analysis establishes the conditions under which either the disease-free or endemic equilibrium governs the long-term behaviour of the epidemic [25–27], as applied in recent stage- and age-structured HIV models using the next-generation matrix and Routh–Hurwitz criteria [28]. Furthermore, sensitivity analysis identifies the epidemiological parameters that exert the greatest influence on disease transmission and persistence [29]. In addition, optimal control theory, based on Pontryagin's Maximum Principle [30, 31], provides a systematic framework for designing intervention strategies that minimize disease prevalence while balancing implementation costs, as demonstrated in recent HIV optimal-control studies using forward–backward sweep implementations [32].

Despite the considerable progress made in HIV modelling, important gaps remain in the existing literature. Current deterministic HIV transmission models generally fall into three broad categories: models that describe detailed disease progression while neglecting adherence-driven resistance dynamics; models that investigate drug resistance without explicitly incorporating infection-stage transmission and treatment-failure pathways; and simplified optimal-control models that do not separately account for treatment adherence, treatment failure, and resistance emergence. For instance, recent unified frameworks combine drug resistance with treatment saturation and vertical transmission [33], and others incorporate treatment failure as a return flow to the aware-infected class [34] or model adherence-driven resistance across multiple strains with treatment switching [35], yet they do not resolve adherence-mediated treatment failure into a distinct compartment linked to a dedicated adherence-support control, which is the mechanism the present model isolates. Consequently, existing modelling frameworks may underestimate the long-term epidemiological consequences of imperfect adherence and the potential role of adherence-support interventions in limiting treatment failure and the emergence of acquired drug resistance [30, 31]. Motivated by these challenges, the present study develops a nonlinear seven-compartment HIV transmission model that simultaneously incorporates infection-stage progression, ART initiation, adherence-mediated treatment failure, and acquired drug resistance within a unified mathematical framework. Unlike previous HIV transmission models, the proposed framework integrates rigorous mathematical analysis, bifurcation analysis, sensitivity analysis, and optimal control within a single epidemiologically consistent and mathematically tractable system.

Specifically, the proposed model is formulated to capture the key epidemiological mechanisms governing HIV transmission, including disease progression, ART initiation, imperfect treatment adherence, treatment failure, and the emergence of drug-resistant HIV strains. The mathematical well-posedness of the model is established by proving the positivity and boundedness of solutions together with the existence of a positively invariant feasible region. The basic reproduction number, $\mathscr{R}_0$, is derived to characterize the threshold dynamics of disease transmission, while the local and global stability properties of the disease-free and endemic equilibria are investigated to describe the long-term behaviour of the system. In addition, normalized sensitivity analysis is performed to identify the parameters that most strongly influence disease persistence. To evaluate effective intervention strategies, an optimal control framework incorporating treatment initiation, adherence-support programmes, and transmission-reduction measures is formulated and analysed using Pontryagin's Maximum Principle. Finally, numerical simulations are performed to provide computational illustrations consistent with the analytical results, examine the qualitative behaviour of the model, and evaluate the proposed intervention strategies under the parameter regimes considered.

The remainder of the paper is organized as follows. Section 2 presents the formulation of the HIV transmission model together with its underlying assumptions. Section 3 establishes the model's mathematical well-posedness. Section 4 derives the basic reproduction number and determines the equilibrium points. Section 5 investigates the local and global stability properties of the equilibria. Section 6 presents the bifurcation and sensitivity analyses, while Section 7 provides numerical simulations illustrating the effects of key epidemiological parameters on the system dynamics. Section 8 formulates and analyzes the optimal control problem. Finally, Section 9 summarizes the main findings and outlines directions for future research.

2. Model formulation

The mathematical HIV-modelling literature reviewed in Section 1 has provided important insights into disease progression, treatment dynamics, and resistance evolution. However, most existing deterministic HIV transmission models investigate these processes separately, and only a limited number of studies simultaneously integrate infection-stage progression, ART uptake, adherence-mediated treatment failure, and acquired drug resistance within a single mathematically tractable framework. Moreover, relatively few existing models are sufficiently comprehensive to permit rigorous stability, bifurcation, sensitivity, and optimal control analyses within a unified mathematical framework. Motivated by these limitations, we develop a unified nonlinear compartmental framework that explicitly captures the interactions among infection-stage progression, ART initiation, adherence-mediated treatment failure, and the emergence of acquired drug resistance within a single epidemiological system.

The proposed framework is designed to balance biological realism with mathematical tractability. Its construction is guided by three principal epidemiological considerations. First, HIV infectivity and disease-induced mortality vary substantially across different stages of infection, necessitating the explicit representation of both early and chronic infectious stages. Second, the framework distinguishes among successful ART treatment, adherence-mediated treatment failure, and acquired drug resistance to mechanistically describe the progression pathway linking imperfect adherence to resistance emergence. Third, a separate AIDS compartment is included to account for advanced disease progression and HIV-related mortality arising from all infected classes. Collectively, these epidemiological considerations naturally motivate a seven-compartment representation of the host population that preserves the principal biological mechanisms while remaining sufficiently tractable for rigorous mathematical analysis.

The total host population at time t, denoted by $\mathscr{N}(t)$, is partitioned into seven mutually exclusive compartments. Susceptible individuals, $\mathscr{S}(t)$, are HIV-negative and at risk of infection. Newly infected individuals enter the acute class $\mathscr{I}_1(t)$, in which high viraemia raises the per-contact transmission probability well above its subsequent levels [5,6], and they later progress to the chronic class $\mathscr{I}_2(t)$, comprising individuals in the established stage of infection who have not yet initiated ART. Those who begin suppressive therapy move into $\mathscr{T}(t)$, where viraemia is effectively suppressed and onward transmission is substantially reduced, in line with the "undetectable = untransmittable" (U = U) principle [3].

The three remaining compartments trace the pathway from imperfect adherence to resistance and advanced disease. Individuals in $\mathscr{F}(t)$ experience treatment failure, that is, virological rebound while still receiving first-line ART, arising primarily from imperfect adherence and, to a lesser extent, from biological breakthrough. Sustained failure allows resistant variants to become established, and the individuals harbouring them constitute the class $\mathscr{R}(t)$. Finally, $\mathscr{A}(t)$ collects individuals with clinical AIDS, representing the advanced stage of infection and aggregating progression from all infected compartments.

The epidemiological interactions among the seven compartments are illustrated schematically in **Figure 1**, where each transition corresponds directly to one of the mechanisms represented in system (2).

$$\mathscr{N}(t) = \mathscr{S}(t) + \mathscr{I}_1(t) + \mathscr{I}_2(t) + \mathscr{T}(t) + \mathscr{F}(t) + \mathscr{R}(t) + \mathscr{A}(t). \tag{1}$$

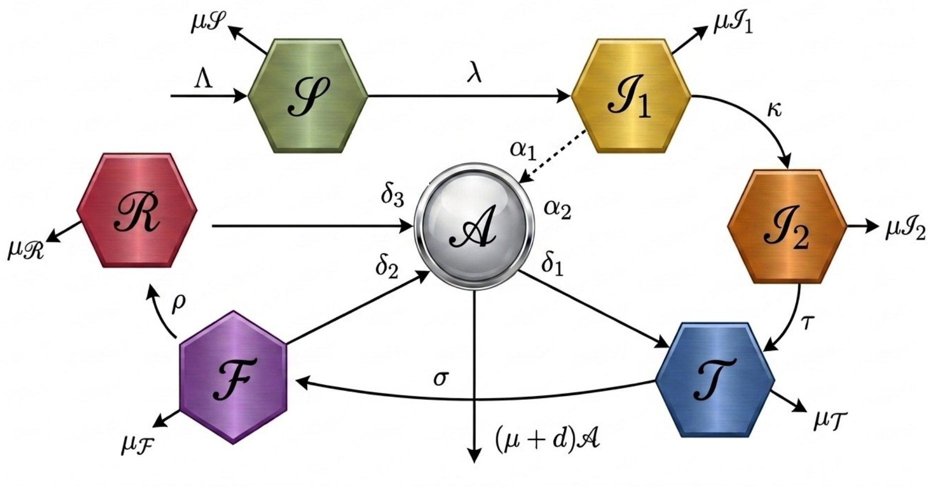

Figure 1. Schematic representation of the proposed seven-compartment HIV transmission model. Solid arrows denote transitions between epidemiological compartments governed by the rate parameters listed in the following table, whereas the dashed arrow represents the force of infection λ, to which all infected compartments contribute with relative infectiousness weights $\{1, \eta_1, \eta_2, \eta_3, \eta_4, \eta_5\}$.

Under the above assumptions, the dynamics of HIV transmission are governed by the following system of nonlinear ordinary differential equations:

$$
\begin{cases}
\dfrac{d\mathscr{S}}{dt} = \Lambda - \lambda\mathscr{S} - \mu\mathscr{S}, \\
\dfrac{d\mathscr{I}_1}{dt} = \lambda\mathscr{S} - (\kappa + \mu + \alpha_1)\mathscr{I}_1, \\
\dfrac{d\mathscr{I}_2}{dt} = \kappa\mathscr{I}_1 - (\tau + \mu + \alpha_2)\mathscr{I}_2, \\
\dfrac{d\mathscr{T}}{dt} = \tau\mathscr{I}_2 - (\sigma + \mu + \delta_1)\mathscr{T}, \\
\dfrac{d\mathscr{F}}{dt} = \sigma\mathscr{T} - (\rho + \mu + \delta_2)\mathscr{F}, \\
\dfrac{d\mathscr{R}}{dt} = \rho\mathscr{F} - (\mu + \delta_3)\mathscr{R}, \\
\dfrac{d\mathscr{A}}{dt} = \alpha_1\mathscr{I}_1 + \alpha_2\mathscr{I}_2 + \delta_1\mathscr{T} + \delta_2\mathscr{F} + \delta_3\mathscr{R} - (\mu + d)\mathscr{A},
\end{cases}
\tag{2}
$$

subject to the initial conditions

$$
\mathscr{S}(0) > 0, \qquad \mathscr{N}(0) > 0, \qquad \mathscr{I}_1(0),\, \mathscr{I}_2(0),\, \mathscr{T}(0),\, \mathscr{F}(0),\, \mathscr{R}(0),\, \mathscr{A}(0) \geq 0.
$$

The force of infection is defined as

$$
\lambda = \frac{\beta\left(\mathscr{I}_1 + \eta_1\mathscr{I}_2 + \eta_2\mathscr{T} + \eta_3\mathscr{F} + \eta_4\mathscr{R} + \eta_5\mathscr{A}\right)}{\mathscr{N}(t)}, \tag{3}
$$

where β denotes the baseline effective transmission rate associated with early-infected individuals, while $\eta_i > 0$ $(i = 1, \ldots, 5)$ are dimensionless modification factors that scale the relative infectiousness of the remaining infected compartments. The term $\alpha_1\mathscr{I}_1$ represents rapid progression from acute HIV infection to AIDS, which occurs relatively infrequently compared with progression through the chronic stage.

Two epidemiologically important features of Equation (3) deserve particular attention. First, $\eta_2 \ll 1$ reflects the substantial reduction in infectiousness achieved through successful ART, consistent with the U = U principle [3]; consequently, individuals receiving effective treatment contribute only minimally to the force of infection. Second, $\eta_4 \approx 1$ reflects the empirical observation that resistance-associated mutations generally do not substantially reduce transmissibility relative to the wild-type virus, allowing drug-resistant individuals to continue contributing to disease transmission at nearly pre-treatment levels.

To clearly define the scope of the subsequent analysis, the assumptions underlying model (2) and the force of infection (3) are stated explicitly. These assumptions are grouped into three categories: structural assumptions, which define the demographic and mixing framework; biological assumptions, which describe the treatment and resistance mechanisms represented; and analytical assumptions, which specify the temporal behaviour of the model parameters.

1. The host population is assumed to mix homogeneously, without explicit age, sex, sexual-risk, or geographical stratification. Behavioural heterogeneity is therefore implicitly incorporated into the aggregate transmission rate β and the relative infectiousness factors η_i. Extensions incorporating population stratification

represent a natural direction for future research.

2. The force of infection λ in Equation (3) is normalized by the total population $\mathcal{N}(t)$, consistent with sexual contact patterns in which an individual's contact rate is assumed to be largely independent of population density.
3. Demographic recruitment occurs exclusively through the susceptible compartment $\mathcal{S}$. Vertical (mother-to-child) transmission is neglected, which is a reasonable approximation for adult-population dynamics but excludes paediatric HIV transmission.
4. The model does not account for viral re-suppression following salvage therapy, treatment re-initiation after disengagement from care, or waning treatment effects that would return individuals to earlier compartments. This assumption considerably simplifies the mathematical analysis and is most appropriate for first-line ART, where spontaneous reversal of treatment failure is relatively uncommon without explicit intervention [36].
5. Drug-resistant variants arise exclusively through treatment failure ($\mathcal{F} \rightarrow \mathcal{R}$). Although individuals in $\mathcal{R}$ contribute to the force of infection in Equation (3), newly infected individuals are not stratified according to resistance status at infection; consequently, transmitted drug resistance is not explicitly represented. In settings where transmitted drug resistance exceeds 10%, this assumption may lead the model to underestimate the overall burden of resistance. Accordingly, the present framework is most applicable to settings in which acquired drug resistance remains the predominant resistance mechanism. Incorporating resistance-stratified infection classes represents an important direction for future model development.
6. The parameter σ combines the two clinically distinct mechanisms responsible for treatment failure, namely imperfect adherence and biological breakthrough, with imperfect adherence assumed to be the dominant mechanism in most empirical settings [7]. This aggregation provides the mechanistic link between σ and the adherence-support control variable u_3 introduced in Section 8.
7. Individuals within each compartment are assumed to experience identical transition rates. In particular, adherence behaviour among treated individuals is considered homogeneous, with individual-level variability incorporated into the parameter σ.
8. All parameters appearing in model (2) and the force of infection (3) are assumed constant over time. Seasonal variation, long-term epidemiological trends, and time-dependent intervention intensities are therefore not considered in the uncontrolled model.

These assumptions represent standard simplifications widely adopted in deterministic compartmental models of HIV transmission [16, 17, 36]. Although each assumption may be relaxed in more detailed modelling frameworks, the present formulation provides a suitable balance between biological realism and mathematical tractability while remaining amenable to rigorous analytical investigation. The analytical properties of the proposed model are examined in the subsequent sections.

For the numerical experiments, the baseline parameter set is obtained by taking the midpoint of each interval reported in **Table 1**, except for parameters represented by a single value. Thus, the simulations use

$$\Lambda = 1, \quad \beta = 0.016, \quad d = 0.03, \quad \kappa = 0.035, \quad \tau = 0.06, \quad \sigma = 0.0125, \quad \rho = 0.0065,$$

together with

$$\eta_1 = 0.65, \quad \eta_2 = 0.20, \quad \eta_3 = 0.55, \quad \eta_4 = 0.85, \quad \eta_5 = 0.65,$$

and the remaining midpoint or fixed values listed in the table. This selection provides a reproducible baseline parameter set while remaining consistent with the biologically plausible ranges reported in the literature and facilitates direct comparison among the numerical experiments presented in subsequent sections.

Table 1. Epidemiological parameters of model (2), together with the biologically plausible ranges used to define the baseline parameter set and their corresponding references. Unless stated otherwise, the midpoint of each reported range is used in the numerical simulations. Unless otherwise indicated, all transition and mortality parameters are expressed in day^{-1}, the recruitment rate Λ is measured in persons per day, and the infectiousness modifiers η_i are dimensionless.

Parameter	**Description**	**Range or baseline value**	**References**
Λ	Recruitment rate into the susceptible compartment $\mathscr{S}$	0.5–1.5	UNAIDS [1]; World Health Organization [2]
μ	Natural mortality rate	3.9×10^{-5}	World Health Organization [2]
d	Disease-induced mortality rate in $\mathscr{A}$	0.01–0.05	World Health Organization [2]
β	Baseline effective transmission rate	0.012–0.020	Liu et al. [16]; Huo and Feng [17]
η_1	Relative infectiousness of $\mathscr{I}_2$ with respect to $\mathscr{I}_1$	0.5–0.8	Nowak and May [5]; Kirschner and Webb [6]
η_2	Relative infectiousness of $\mathscr{T}$	0.1–0.3	Granich et al. [3]
η_3	Relative infectiousness of $\mathscr{F}$	0.4–0.7	Brauer [36]
η_4	Relative infectiousness of $\mathscr{R}$	0.7–1.0	Blower et al. [7]
η_5	Relative infectiousness of $\mathscr{A}$	0.5–0.8	Kirschner and Webb [6]
κ	Progression rate from $\mathscr{I}_1$ to $\mathscr{I}_2$	0.02–0.05	Nowak and May [5]; Kirschner and Webb [6]
α_1	Progression rate from $\mathscr{I}_1$ to $\mathscr{A}$	0.0003–0.001	Kirschner and Webb [6]; Huo and Feng [17]
α_2	Progression rate from $\mathscr{I}_2$ to $\mathscr{A}$	0.001–0.003	Kirschner and Webb [6]; Huo and Feng [17]
δ_1	Progression rate from $\mathscr{T}$ to $\mathscr{A}$	0.0005	Granich et al. [3]
δ_2	Progression rate from $\mathscr{F}$ to $\mathscr{A}$	0.004–0.01	Brauer [36]
δ_3	Progression rate from $\mathscr{R}$ to $\mathscr{A}$	0.005–0.01	Brauer [36]
τ	ART initiation rate ($\mathscr{I}_2 \to \mathscr{T}$)	0.04–0.08	Granich et al. [3]
σ	Treatment-failure rate ($\mathscr{T} \to \mathscr{F}$)	0.005–0.02	Blower et al. [7]
ρ	Acquired drug-resistance rate ($\mathscr{F} \to \mathscr{R}$)	0.003–0.01	Blower et al. [7]

The baseline parameter values are derived from literature-reported ranges and were not estimated by fitting the model to a specific epidemiological dataset. Accordingly, the numerical results presented below should be interpreted as qualitative, model-based illustrations of the system dynamics under biologically plausible parameter values rather than as calibrated quantitative predictions for any particular population or geographical setting.

3. Positivity and boundedness

Theorem 1 (Positivity and boundedness)**.** *For non-negative initial conditions of the state variables, system* (2) *admits a unique global solution. Furthermore, the* *non-negative orthant is positively invariant, and all solutions are ultimately bounded. In addition, the feasible region*

$$\Omega = \left\{(\mathscr{S}, \mathscr{I}_1, \mathscr{I}_2, \mathscr{T}, \mathscr{F}, \mathscr{R}, \mathscr{A}) \in \mathbb{R}^7_+ : 0 < \mathscr{N} \le \frac{\Lambda}{\mu}\right\}$$

is positively invariant for all solutions that originate within it.

Proof. Consider the force of infection, given by

$$\lambda = \frac{\beta\big(\mathscr{I}_1 + \eta_1\mathscr{I}_2 + \eta_2\mathscr{T} + \eta_3\mathscr{F} + \eta_4\mathscr{R} + \eta_5\mathscr{A}\big)}{\mathscr{N}}.$$

For $\mathscr{N} > 0$, this expression is continuously differentiable. Hence, the right-hand side of system (2) is locally Lipschitz in the region

$$\mathbb{R}^7_+ \cap \{\mathscr{N} > 0\}.$$

It therefore follows from the Picard–Lindelöf theorem [37] that system (2) possesses a unique local solution defined on a maximal interval $[0, t_{\max})$.

We now establish the positivity of the solutions. On the boundary hyperplanes of the non-negative orthant, the vector field satisfies

$$\left.\frac{d\mathscr{S}}{dt}\right|_{\mathscr{S}=0} = \Lambda \ge 0, \qquad \left.\frac{d\mathscr{I}_1}{dt}\right|_{\mathscr{I}_1=0} = \lambda\mathscr{S} \ge 0,$$

$$\left.\frac{d\mathscr{I}_2}{dt}\right|_{\mathscr{I}_2=0} = \kappa\mathscr{I}_1 \ge 0, \qquad \left.\frac{d\mathscr{T}}{dt}\right|_{\mathscr{T}=0} = \tau\mathscr{I}_2 \ge 0,$$

$$\left.\frac{d\mathscr{F}}{dt}\right|_{\mathscr{F}=0} = \sigma\mathscr{T} \ge 0, \qquad \left.\frac{d\mathscr{R}}{dt}\right|_{\mathscr{R}=0} = \rho\mathscr{F} \ge 0,$$

and

$$\left.\frac{d\mathscr{A}}{dt}\right|_{\mathscr{A}=0} = \alpha_1\mathscr{I}_1 + \alpha_2\mathscr{I}_2 + \delta_1\mathscr{T} + \delta_2\mathscr{F} + \delta_3\mathscr{R} \ge 0.$$

These inequalities show that, on each boundary face of $\mathbb{R}^7_+$, the vector field is directed toward the non-negative region or is tangent to its boundary. Consequently, Nagumo's positive invariance theorem for ordinary differential equations [37] guarantees that $\mathbb{R}^7_+$ is positively invariant.

To establish boundedness, we sum all equations of system (2) to obtain

$$\frac{d\mathscr{N}}{dt} = \Lambda - \mu\mathscr{N} - d\mathscr{A} \le \Lambda - \mu\mathscr{N}.$$

Applying the comparison theorem [38] to the auxiliary equation

$$\dot{Y} = \Lambda - \mu Y,$$

we obtain

$$\mathscr{N}(t) \le \mathscr{N}(0)e^{-\mu t} + \frac{\Lambda}{\mu}\left(1 - e^{-\mu t}\right).$$

This implies that

$$\limsup_{t\to\infty} \mathcal{N}(t) \leq \frac{\Lambda}{\mu}.$$

Therefore, if

$$\mathcal{N}(0) \leq \frac{\Lambda}{\mu},$$

then

$$\mathcal{N}(t) \leq \frac{\Lambda}{\mu},$$

If instead

$$\mathcal{N}(0) > \frac{\Lambda}{\mu},$$

the comparison estimate gives

$$\mathcal{N}(t) \leq \frac{\Lambda}{\mu} + \left(\mathcal{N}(0) - \frac{\Lambda}{\mu}\right) e^{-\mu t}.$$

Thus, for every $\varepsilon > 0$, there exists $t_\varepsilon > 0$ such that

$$\mathcal{N}(t) \leq \frac{\Lambda}{\mu} + \varepsilon, \qquad t \geq t_\varepsilon.$$

As a result, every trajectory approaches the region Ω asymptotically, and all solutions are ultimately bounded. Moreover, if a trajectory originates in Ω, then

$$\mathcal{N}(t) \leq \frac{\Lambda}{\mu} \qquad \text{for all } t \geq 0,$$

continues to hold throughout its evolution. Therefore, a solution starting in Ω cannot leave this region, which establishes the positive invariance of Ω.

The non-negativity of the state variables, together with their boundedness over every finite time interval, rules out the possibility of finite-time blow-up. It follows that the maximal existence time satisfies

$$t_{\max} = \infty.$$

Consequently, the unique local solution obtained above continues uniquely for every $t \geq 0$, and is therefore a global solution. □

4. Basic reproduction number

We now determine the equilibrium configurations associated with the HIV transmission system. Particular attention is given to the basic reproduction number $\mathscr{R}_0$, which is obtained through the next-generation matrix (NGM) framework. The stability behavior of the corresponding equilibrium states is subsequently examined from both local and global perspectives.

In the absence of infection, system (2) possesses the disease-free equilibrium, denoted by $\mathcal{E}_0$, with the form

$$\mathcal{E}_0 = \left(\mathcal{S}^0, 0, 0, 0, 0, 0, 0\right) = \left(\frac{\Lambda}{\mu}, 0, 0, 0, 0, 0, 0\right), \tag{4}$$

and this equilibrium is located on the boundary of the biologically admissible region Ω. At $\mathcal{E}_0$, all infected compartments vanish, so the entire population belongs to the susceptible class. Accordingly,

$$\mathcal{N}^0 = \mathcal{S}^0 = \frac{\Lambda}{\mu},$$

and consequently, we have

$$\frac{\mathcal{S}^0}{\mathcal{N}^0} = 1.$$

The basic reproduction number, $\mathcal{R}_0$, is derived using the next-generation matrix (NGM) approach developed by Diekmann et al. [23] and van den Driessche and Watmough [24]. For the application of the next-generation matrix method, the infected subsystem consists of the six epidemiologically infected compartments

$$\mathbf{x} = (\mathcal{I}_1, \mathcal{I}_2, \mathcal{T}, \mathcal{F}, \mathcal{R}, \mathcal{A})^\top,$$

whose dynamics can be written as

$$\dot{\mathbf{x}} = \mathcal{F}(\mathbf{x}) - \mathcal{V}(\mathbf{x}),$$

where

$$\mathcal{F}(\mathbf{x}) = \begin{pmatrix} \lambda\mathcal{S} \\ 0 \\ 0 \\ 0 \\ 0 \\ 0 \end{pmatrix}, \qquad \mathcal{V}(\mathbf{x}) = \begin{pmatrix} (\kappa + \mu + \alpha_1)\mathcal{I}_1 \\ (\tau + \mu + \alpha_2)\mathcal{I}_2 - \kappa\mathcal{I}_1 \\ (\sigma + \mu + \delta_1)\mathcal{T} - \tau\mathcal{I}_2 \\ (\rho + \mu + \delta_2)\mathcal{F} - \sigma\mathcal{T} \\ (\mu + \delta_3)\mathcal{R} - \rho\mathcal{F} \\ (\mu + d)\mathcal{A} - \alpha_1\mathcal{I}_1 - \alpha_2\mathcal{I}_2 - \delta_1\mathcal{T} - \delta_2\mathcal{F} - \delta_3\mathcal{R} \end{pmatrix},$$

with the force of infection λ given by Equation (3). The vector $\mathcal{F}$ represents the rates at which new infections enter the infected subsystem, whereas $\mathcal{V}$ accounts for all other transition processes, including disease progression, treatment initiation, treatment failure, resistance emergence, and disease-induced removal within the infected subsystem.

Linearizing the infected subsystem about the disease-free equilibrium $\mathcal{E}_0$ and using

$$\frac{\mathcal{S}^0}{\mathcal{N}^0} = 1,$$

the Jacobian matrices

$$F = D_{\mathbf{x}}\mathcal{F}\big|_{\mathcal{E}_0}, \qquad V = D_{\mathbf{x}}\mathcal{V}\big|_{\mathcal{E}_0},$$

are given by

$$F = \begin{pmatrix} \beta & \beta\eta_1 & \beta\eta_2 & \beta\eta_3 & \beta\eta_4 & \beta\eta_5 \\ 0 & 0 & 0 & 0 & 0 & 0 \\ 0 & 0 & 0 & 0 & 0 & 0 \\ 0 & 0 & 0 & 0 & 0 & 0 \\ 0 & 0 & 0 & 0 & 0 & 0 \\ 0 & 0 & 0 & 0 & 0 & 0 \end{pmatrix}, \quad V = \begin{pmatrix} a_1 & 0 & 0 & 0 & 0 & 0 \\ -\kappa & a_2 & 0 & 0 & 0 & 0 \\ 0 & -\tau & a_3 & 0 & 0 & 0 \\ 0 & 0 & -\sigma & a_4 & 0 & 0 \\ 0 & 0 & 0 & -\rho & a_5 & 0 \\ -\alpha_1 & -\alpha_2 & -\delta_1 & -\delta_2 & -\delta_3 & a_6 \end{pmatrix}, \tag{5}$$

where

$$a_1 = \kappa + \mu + \alpha_1, \qquad a_2 = \tau + \mu + \alpha_2, \qquad a_3 = \sigma + \mu + \delta_1,$$

$$a_4 = \rho + \mu + \delta_2, \qquad a_5 = \mu + \delta_3, \qquad a_6 = \mu + d.$$

The basic reproduction number is defined as

$$\mathscr{R}_0 = \varrho(FV^{-1}),$$

where $\varrho(\cdot)$ denotes the spectral radius. Because V is lower triangular, V^{-1} is also lower triangular with diagonal entries $1/a_i$, and the entries of its first column are obtained by forward substitution. Since only the first row of F is non-zero, the product FV^{-1} also has only its first row non-zero and is therefore a rank-one matrix. Consequently, its only potentially non-zero eigenvalue is equal to its trace, namely the $(1,1)$ entry, which is obtained as the inner product of the first row of F with the first column of V^{-1}. Consequently, we have

$$\mathscr{R}_0 = \beta\big(\mathscr{R}_{\text{prog}} + \mathscr{R}_{\text{AIDS}}\big), \tag{6}$$

where the progression and AIDS-mediated contributions are

$$\mathscr{R}_{\text{prog}} = \frac{1}{a_1} + \frac{\eta_1\kappa}{a_1a_2} + \frac{\eta_2\kappa\tau}{a_1a_2a_3} + \frac{\eta_3\kappa\tau\sigma}{a_1a_2a_3a_4} + \frac{\eta_4\kappa\tau\sigma\rho}{a_1a_2a_3a_4a_5}, \tag{7}$$

$$\mathscr{R}_{\text{AIDS}} = \frac{\eta_5}{a_6}\left(\frac{\alpha_1}{a_1} + \frac{\alpha_2\kappa}{a_1a_2} + \frac{\delta_1\kappa\tau}{a_1a_2a_3} + \frac{\delta_2\kappa\tau\sigma}{a_1a_2a_3a_4} + \frac{\delta_3\kappa\tau\sigma\rho}{a_1a_2a_3a_4a_5}\right). \tag{8}$$

Grouping each AIDS-mediated pathway with its corresponding disease-progression pathway yields the equivalent compact representation

$$\begin{aligned} \mathscr{R}_0 = \beta\Bigg[& \frac{1}{a_1}\left(1 + \frac{\eta_5\alpha_1}{a_6}\right) + \frac{\kappa}{a_1a_2}\left(\eta_1 + \frac{\eta_5\alpha_2}{a_6}\right) \\ & + \frac{\kappa\tau}{a_1a_2a_3}\left(\eta_2 + \frac{\eta_5\delta_1}{a_6}\right) + \frac{\kappa\tau\sigma}{a_1a_2a_3a_4}\left(\eta_3 + \frac{\eta_5\delta_2}{a_6}\right) \\ & + \frac{\kappa\tau\sigma\rho}{a_1a_2a_3a_4a_5}\left(\eta_4 + \frac{\eta_5\delta_3}{a_6}\right)\Bigg]. \end{aligned} \tag{9}$$

Each term in Equations (7) and (8) admits the standard interpretation of

transmission rate × probability of reaching the compartment × mean residence time,

scaled by the relative infectiousness of the corresponding compartment through the modification factor η_i.

The derived basic reproduction number has the following epidemiological interpretation.

- The term $\frac{\beta}{a_1}$, represents the contribution from early-infected individuals. An individual entering compartment $\mathcal{I}_1$ remains there for an average duration of $1/a_1$ and transmits infection at the baseline rate β.
- The term $\frac{\beta\eta_1\kappa}{a_1 a_2}$, represents the contribution from the chronically infected compartment. The factor $\frac{\kappa}{a_1}$, is the probability that an individual in $\mathcal{I}_1$ progresses to $\mathcal{I}_2$ before leaving the compartment through other routes, while $\frac{1}{a_2}$, denotes the average residence time in $\mathcal{I}_2$. The modification factor η_1 scales the infectiousness of chronically infected individuals relative to those in the early stage of infection.
- The remaining terms in $\mathcal{R}_{\text{prog}}$ describe successive disease progression through the treated ($\mathcal{T}$), treatment-failure ($\mathcal{F}$), and drug-resistant ($\mathcal{R}$) compartments. Each additional factor represents the conditional probability of progressing to the next compartment together with the corresponding mean residence time.
- The quantity $\mathcal{R}_{\text{AIDS}}$ accounts for transmission arising from individuals in the AIDS compartment. Individuals may enter $\mathcal{A}$ from any infected compartment through the progression rates α_1, α_2, δ_1, δ_2, and δ_3. Each corresponding pathway contributes according to the cumulative probability of reaching the AIDS compartment and the average residence time $1/a_6$, scaled by the relative infectiousness factor η_5.

For biologically plausible parameter values, the chronic-stage contribution $\frac{\beta\eta_1\kappa}{a_1 a_2}$, is generally expected to constitute one of the dominant components of $\mathcal{R}_0$, primarily because individuals typically remain in the chronic stage considerably longer than in the acute stage. By contrast, the treatment-related contributions are substantially attenuated by the reduced infectiousness of effectively treated individuals ($\eta_2 \ll 1$), reflecting the suppressive effect of ART on viral transmission.

5. Stability analysis

In this section, we investigate the stability of the disease-free and endemic equilibria of the proposed model.

Theorem 2. *The disease-free equilibrium $\mathcal{E}_0$ of system* (2) *is locally asymptotically stable whenever $\mathcal{R}_0 < 1$ and unstable whenever $\mathcal{R}_0 > 1$.*

The local stability of the disease-free equilibrium follows directly from the next-generation matrix construction presented in Section 4. We now extend this local result to establish the global asymptotic stability of the disease-free equilibrium.

Theorem 3. *The disease-free equilibrium*

$$\mathcal{E}_0 = \left(\frac{\Lambda}{\mu}, 0, \dots, 0\right),$$

of system (2) *is globally asymptotically stable in the biologically feasible region*

$$\Omega = \left\{ \mathbf{x} \in \mathbb{R}_+^7 : 0 < \mathcal{N} \leq \frac{\Lambda}{\mu} \right\},$$

whenever $\mathcal{R}_0 < 1$.

Proof. We establish global asymptotic stability using the framework of Castillo–Chavez, Feng, and Huang [26]. Decompose the state variables as

$$X = \mathcal{S}, \qquad Z = (\mathcal{I}_1, \mathcal{I}_2, \mathcal{T}, \mathcal{F}, \mathcal{R}, \mathcal{A})^\top,$$

and rewrite system (2) as

$$\dot{X} = \mathcal{F}_1(X, Z), \qquad \dot{Z} = \mathcal{G}(X, Z).$$

The Castillo-Chavez theorem guarantees the global asymptotic stability of $\mathcal{E}_0$ provided that the following conditions hold.

Hypothesis 1 (H1)**.** *For*

$$\dot{X} = \mathcal{F}_1(X, 0),$$

the equilibrium

$$X^* = \frac{\Lambda}{\mu},$$

is globally asymptotically stable.

Hypothesis 2 (H2)**.** *The infected subsystem satisfies*

$$\mathcal{G}(X, Z) = AZ - \widehat{\mathcal{G}}(X, Z),$$

where

$$\widehat{\mathcal{G}}(X, Z) \geq 0,$$

for all

$$(X, Z) \in \Omega,$$

and

$$A = D_Z \mathcal{G}(X^*, 0),$$

is a Metzler matrix.

Verification of H1. Setting $Z = 0$ yields

$$\dot{X} = \Lambda - \mu X,$$

whose unique equilibrium

$$X^* = \frac{\Lambda}{\mu},$$

is globally asymptotically stable.

Verification of H2. A direct computation yields

$$A = F - V,$$

where the matrices F and V are defined in Equation (5). Because F has non-negative entries and V is a nonsingular M-matrix, the matrix A has the Metzler property. Furthermore, Theorem 2 of van den Driessche and Watmough [24] implies that

$$s(A) < 0$$

if and only if

$$\mathscr{R}_0 < 1.$$

The residual vector

$$\widehat{\mathcal{G}} = AZ - \mathcal{G}(X, Z),$$

has only one non-zero component,

$$\widehat{\mathcal{G}}_1(X, Z) = \beta\left(\mathscr{I}_1 + \eta_1\mathscr{I}_2 + \eta_2\mathscr{T} + \eta_3\mathscr{F} + \eta_4\mathscr{R} + \eta_5\mathscr{A}\right)\left(1 - \frac{\mathcal{S}}{\mathcal{N}}\right),$$

with

$$\widehat{\mathcal{G}}_i = 0, \qquad i = 2, \ldots, 6.$$

Within the biologically feasible set Ω, every state variable is non-negative. In addition, the susceptible population cannot exceed the total population, so that

$$\mathcal{S} \leq \mathcal{N},$$

it follows that

$$1 - \frac{\mathcal{S}}{\mathcal{N}} \geq 0,$$

and consequently,

$$\widehat{\mathcal{G}} \geq 0.$$

Thus, both conditions H1 and H2 required by the Castillo–Chavez theorem are fulfilled. It follows that, whenever $\mathscr{R}_0 < 1$, the disease-free equilibrium $\mathcal{E}_0$ is globally asymptotically stable throughout the feasible region Ω.

□

Endemic equilibrium

Next, we investigate the endemic equilibrium of the system. When $\mathscr{R}_0 > 1$, the disease-free equilibrium loses stability, and a positive endemic equilibrium

$$\mathcal{E}^* = (\mathcal{S}^*, \mathscr{I}_1^*, \mathscr{I}_2^*, \mathscr{T}^*, \mathscr{F}^*, \mathscr{R}^*, \mathscr{A}^*)$$

may exist. The equilibrium solutions are obtained by setting the right-hand side of system (2) to zero, the lower-triangular structure of the infected subsystem allows us to express every infected compartment in terms of $\mathcal{I}_1^*$:

$$\mathcal{I}_2^* = q_2\mathcal{I}_1^*, \quad \mathcal{T}^* = q_3\mathcal{I}_1^*, \quad \mathcal{F}^* = q_4\mathcal{I}_1^*, \quad \mathcal{R}^* = q_5\mathcal{I}_1^*, \quad \mathcal{A}^* = q_6\mathcal{I}_1^*, \tag{10}$$

where

$$q_2 = \frac{\kappa}{a_2}, \qquad q_3 = \frac{\kappa\tau}{a_2a_3}, \qquad q_4 = \frac{\kappa\tau\sigma}{a_2a_3a_4}, \qquad q_5 = \frac{\kappa\tau\sigma\rho}{a_2a_3a_4a_5}, \tag{11}$$

$$q_6 = \frac{1}{a_6}\left(\alpha_1 + \alpha_2 q_2 + \delta_1 q_3 + \delta_2 q_4 + \delta_3 q_5\right).$$

Here, each $q_i > 0$ represents the equilibrium size of the corresponding downstream infected compartment relative to $\mathcal{I}_1^*$. These coefficients are determined by the sequential progression rates and the average residence times within the intermediate compartments.

The total equilibrium population is

$$\mathcal{N}^* = \mathcal{S}^* + Q\mathcal{I}_1^*,$$

where

$$Q = 1 + q_2 + q_3 + q_4 + q_5 + q_6 > 0,$$

and the equilibrium force of infection is

$$\lambda^* = \frac{\beta P \mathcal{I}_1^*}{\mathcal{N}^*}, \qquad P = 1 + \eta_1 q_2 + \eta_2 q_3 + \eta_3 q_4 + \eta_4 q_5 + \eta_5 q_6. \tag{12}$$

Substituting the definitions of P and a_1 into Equations (6)–(8) yields

$$\mathcal{R}_0 = \frac{\beta P}{a_1}. \tag{13}$$

Together with

$$\mathcal{S}^* = \frac{\Lambda}{\mu + \lambda^*}, \qquad \mathcal{I}_1^* = \frac{\lambda^* \mathcal{S}^*}{a_1},$$

Equation (12) reduces to the linear consistency condition

$$a_1 + Q\lambda^* = \beta P,$$

whose unique solution is

$$\lambda^* = \frac{\beta P - a_1}{Q} = \frac{a_1(\mathcal{R}_0 - 1)}{Q}. \tag{14}$$

Theorem 4. *System* (2) *admits a unique endemic equilibrium* $\mathcal{E}^* \in \mathring{\Omega}$ *if and only if* $\mathcal{R}_0 > 1$. *The components of* $\mathcal{E}^*$ *are determined by Equations* (10) *and* (11)*, together with*

$$\mathcal{S}^* = \frac{\Lambda}{\mu + \lambda^*}, \qquad \mathcal{I}_1^* = \frac{\lambda^* \mathcal{S}^*}{a_1},$$

where λ^* *is given by Equation* (14).

Theorem 4 establishes the existence and uniqueness of the endemic equilibrium $\mathcal{E}^* \in \Omega$, with all infected compartments remaining positive whenever $\mathcal{R}_0 > 1$. We next investigate its local asymptotic stability by means of direct linearization and the Routh–Hurwitz criterion applied to the full 7×7 Jacobian matrix.

This approach is adopted in place of a Volterra–Lyapunov argument because the force of infection (3) is frequency dependent through the factor $1/\mathcal{N}(t)$, preventing the standard telescoping cancellation from producing an explicitly non-positive remainder without a complete derivation of all cross terms. Moreover, the chain structure of system (2) does not simplify such a derivation sufficiently to obtain a tractable Lyapunov function.

Local stability of the endemic equilibrium

Theorem 5. *Suppose that $\mathcal{R}_0 > 1$, and let $\mathcal{E}^* \in \mathring{\Omega}$ denote the unique endemic equilibrium of system* (2)*. Let*

$$\Phi(\xi) = \xi^7 + b_1\xi^6 + b_2\xi^5 + b_3\xi^4 + b_4\xi^3 + b_5\xi^2 + b_6\xi + b_7,$$

be the characteristic polynomial of the Jacobian matrix $J^* = J(\mathcal{E}^*)$. Then $\mathcal{E}^*$ is locally asymptotically stable if and only if

$$\Delta_i > 0, \qquad i = 1, 2, \ldots, 7,$$

where Δ_i denotes the ith leading principal minor of the Hurwitz matrix associated with $\Phi(\xi)$.

Proof. Order the state variables as

$$(\mathcal{S}, \mathcal{I}_1, \mathcal{I}_2, \mathcal{T}, \mathcal{F}, \mathcal{R}, \mathcal{A}).$$

The local dynamics of system (2) in a neighbourhood of $\mathcal{E}^*$ are governed by the linearized system

$$\dot{X} = J^* X,$$

where J^* is the 7×7 Jacobian matrix of system (2) evaluated at $\mathcal{E}^*$.

Define the equilibrium total population by

$$\mathcal{N}^* = \mathcal{S}^* + \mathcal{I}_1^* + \mathcal{I}_2^* + \mathcal{T}^* + \mathcal{F}^* + \mathcal{R}^* + \mathcal{A}^*.$$

For notational convenience in the linearization below, define the stage-specific transmission rates

$$\beta_1 := \beta, \;\; \beta_2 := \beta\eta_1, \;\; \beta_3 := \beta\eta_2, \;\; \beta_4 := \beta\eta_3, \;\; \beta_5 := \beta\eta_4, \;\; \beta_6 := \beta\eta_5,$$

so that the equilibrium force of infection can be written as

$$\lambda^* = \frac{\beta_1\mathcal{I}_1^* + \beta_2\mathcal{I}_2^* + \beta_3\mathcal{T}^* + \beta_4\mathcal{F}^* + \beta_5\mathcal{R}^* + \beta_6\mathcal{A}^*}{\mathcal{N}^*} > 0, \tag{15}$$

which coincides with the force of infection (3) evaluated at the endemic equilibrium $\mathcal{E}^*$.

Let $\tilde{\lambda}$ denote the force-of-infection function and define

$$\Lambda_k := \mathcal{S}^* \frac{\partial \tilde{\lambda}}{\partial X_k}\bigg|_{\mathcal{E}^*},$$

for each compartment X_k. A direct computation using the quotient rule yields

$$\Lambda_{\mathcal{S}} = -\frac{\lambda^* \mathcal{S}^*}{\mathcal{N}^*} < 0, \qquad \Lambda_{\mathcal{I}_j} = \frac{(\beta_j - \lambda^*)\mathcal{S}^*}{\mathcal{N}^*}, \quad j = 1, 2, \tag{16}$$

$$\Lambda_{\mathcal{T}} = \frac{(\beta_3 - \lambda^*)\mathcal{S}^*}{\mathcal{N}^*}, \qquad \Lambda_{\mathcal{F}} = \frac{(\beta_4 - \lambda^*)\mathcal{S}^*}{\mathcal{N}^*}, \tag{17}$$

$$\Lambda_{\mathcal{R}} = \frac{(\beta_5 - \lambda^*)\mathcal{S}^*}{\mathcal{N}^*}, \qquad \Lambda_{\mathcal{A}} = \frac{(\beta_6 - \lambda^*)\mathcal{S}^*}{\mathcal{N}^*}. \tag{18}$$

The Jacobian matrix J^* admits the partitioned representation

$$J^* = \begin{pmatrix} B & \mathbf{q} \\ \mathbf{r} & C \end{pmatrix}, \tag{19}$$

where $B \in \mathbb{R}^{2\times 2}$ governs the variables $(\mathcal{S}, \mathcal{I}_1)$, $C \in \mathbb{R}^{5\times 5}$ governs $(\mathcal{I}_2, \mathcal{T}, \mathcal{F}, \mathcal{R}, \mathcal{A})$, and $\mathbf{q} \in \mathbb{R}^{2\times 5}$ and $\mathbf{r} \in \mathbb{R}^{5\times 2}$ represent the coupling matrices arising from the frequency-dependent force of infection. Since both $\mathbf{q}$ and $\mathbf{r}$ are generally non-zero, the full Jacobian matrix J^* is not block triangular. Consequently, no spectral factorization of the form

$$\det(\xi I - J^*) = \det(\xi I_2 - B)\ \det(\xi I_5 - C),$$

is valid. Therefore, the stability of the diagonal blocks alone is insufficient to establish the stability of J^*, and the analysis must instead be carried out using the full 7×7 characteristic polynomial.

Explicitly,

$$B = \begin{pmatrix} -(\lambda^* + \mu) - \Lambda_{\mathcal{S}} & -\Lambda_{\mathcal{I}_1} \\ \lambda^* + \Lambda_{\mathcal{S}} & -a_1 + \Lambda_{\mathcal{I}_1} \end{pmatrix}, \tag{20}$$

where $a_1 = \mu + \kappa + \alpha_1$ denotes the total outflow rate from $\mathcal{I}_1$. The coupling matrices are

$$\mathbf{q} = \begin{pmatrix} -\Lambda_{\mathcal{I}_2} & -\Lambda_{\mathcal{T}} & -\Lambda_{\mathcal{F}} & -\Lambda_{\mathcal{R}} & -\Lambda_{\mathcal{A}} \\ \Lambda_{\mathcal{I}_2} & \Lambda_{\mathcal{T}} & \Lambda_{\mathcal{F}} & \Lambda_{\mathcal{R}} & \Lambda_{\mathcal{A}} \end{pmatrix},$$

and

$$\mathbf{r} = \begin{pmatrix} 0 & \kappa \\ 0 & 0 \\ 0 & 0 \\ 0 & 0 \\ 0 & \alpha_1 \end{pmatrix}.$$

$$C = \begin{pmatrix} -a_2 & 0 & 0 & 0 & 0 \\ \tau & -a_3 & 0 & 0 & 0 \\ 0 & \sigma & -a_4 & 0 & 0 \\ 0 & 0 & \rho & -a_5 & 0 \\ \alpha_2 & \delta_1 & \delta_2 & \delta_3 & -a_6 \end{pmatrix}, \tag{21}$$

where a_j are the corresponding total outflow rates defined in Section 2. The endemic equilibrium $\mathcal{E}^*$ is locally asymptotically stable if and only if all eigenvalues of J^* have strictly negative real parts. These eigenvalues are precisely the roots of the characteristic polynomial

$$\Phi(\xi) = \det(\xi I - J^*) = \xi^7 + b_1\xi^6 + b_2\xi^5 + b_3\xi^4 + b_4\xi^3 + b_5\xi^2 + b_6\xi + b_7.$$

The coefficients $b_1, \ldots, b_7$ depend explicitly on the model parameters and the endemic equilibrium coordinates. Their closed-form expressions are algebraically lengthy and therefore omitted for brevity. By the Routh–Hurwitz criterion, all roots of $\Phi(\xi)$ have strictly negative real parts if and only if all leading principal minors of the associated Hurwitz matrix

$$H = \begin{pmatrix} b_1 & b_3 & b_5 & b_7 & 0 & 0 & 0 \\ 1 & b_2 & b_4 & b_6 & 0 & 0 & 0 \\ 0 & b_1 & b_3 & b_5 & b_7 & 0 & 0 \\ 0 & 1 & b_2 & b_4 & b_6 & 0 & 0 \\ 0 & 0 & b_1 & b_3 & b_5 & b_7 & 0 \\ 0 & 0 & 1 & b_2 & b_4 & b_6 & 0 \\ 0 & 0 & 0 & b_1 & b_3 & b_5 & b_7 \end{pmatrix}, \tag{22}$$

are strictly positive,

$$\Delta_i > 0, \qquad i = 1, 2, \ldots, 7. \tag{23}$$

Under conditions (23), every root of $\Phi(\xi)$ lies in the open left half-plane. Hence, all eigenvalues of J^* have strictly negative real parts, and the classical linearization theorem implies that $\mathcal{E}^*$ is locally asymptotically stable. □

Remark 1. *The symbolic expressions for the Hurwitz determinants $\Delta_1, \ldots, \Delta_7$ are algebraically lengthy and are therefore omitted. For the baseline parameter set used in the numerical analysis, the eigenvalues of the Jacobian matrix J^* were computed directly and were found to have strictly negative real parts. Hence, the Routh–Hurwitz stability criterion of Theorem 5 is satisfied for this specific parameter set. This numerical verification should not be interpreted as a proof of local asymptotic stability for every parameter set satisfying $\mathscr{R}_0 > 1$.*

Remark 2. *The preceding analysis establishes only local asymptotic stability of the endemic equilibrium. Since the conclusion follows from the linearization of the system at $\mathcal{E}^*$, it guarantees convergence only for initial conditions lying in a sufficiently small neighbourhood of the equilibrium. Establishing global asymptotic stability for $\mathscr{R}_0 > 1$ remains an open problem for the present model. The frequency-dependent incidence with the time-varying denominator $\mathcal{N}(t)$ precludes the direct application of existing graph-theoretic Lyapunov methods [39]. Nevertheless, the numerical simulations presented in Section 7 show convergence toward $\mathcal{E}^*$ for the initial conditions examined. This provides parameter-specific numerical evidence of attraction toward the endemic equilibrium but does not establish global attraction. A rigorous global stability analysis* *therefore remains an open problem for the present model.*

6. Bifurcation and sensitivity analysis

In this section, we investigate the local bifurcation behaviour of the proposed HIV transmission model and subsequently perform a sensitivity analysis to identify the parameters that most strongly influence disease transmission.

Theorem 5 provides a Routh–Hurwitz criterion for the local asymptotic stability of the endemic equilibrium $\mathcal{E}^*$ when $\mathscr{R}_0 > 1$. For the baseline parameter set considered below, local stability is verified numerically through direct computation of the Jacobian eigenvalues. A complementary question concerns the nature of the bifurcation at the threshold $\mathscr{R}_0 = 1$. Specifically, we determine whether the endemic equilibrium emerging as $\mathscr{R}_0$ crosses unity appears continuously (forward bifurcation) or exhibits a discontinuous transition with possible bistability (backward bifurcation). The Routh–Hurwitz criterion establishes stability away from the threshold but does not determine the type of bifurcation. Therefore, we employ the centre-manifold theorem of Castillo-Chavez and Song [25], which provides the standard framework for characterizing local bifurcation behaviour in compartmental epidemic models.

Taking the effective transmission rate β as the bifurcation parameter, the critical value $\beta^* = \frac{a_1}{P}$, obtained by setting $\mathscr{R}_0 = 1$ in Equation (13), corresponds to the bifurcation point. At $(\mathcal{E}_0, \beta^*)$, the Jacobian matrix possesses a simple zero eigenvalue, while all remaining eigenvalues have negative real parts. Let

$$\mathbf{w} = (w_1, \ldots, w_7)^\top, \qquad \mathbf{v} = (v_1, \ldots, v_7),$$

represent the corresponding right and left eigenvectors, respectively, normalized such that $\mathbf{v}\mathbf{w} = 1$.

To determine the local dynamics near the threshold $\mathscr{R}_0 = 1$, we employ the centre-manifold approach developed by Castillo-Chavez and Song [25]. Using this approach, both the direction of the bifurcation and the local stability of the resulting endemic equilibrium can be determined.

$$\mathcal{A} = \sum_{k,i,j=1}^{7} v_k w_i w_j \frac{\partial^2 f_k}{\partial x_i \partial x_j}(\mathcal{E}_0, \beta^*),$$

and

$$\mathcal{B} = \sum_{k,i=1}^{7} v_k w_i \frac{\partial^2 f_k}{\partial x_i \partial \beta}(\mathcal{E}_0, \beta^*),$$

where f_k denotes the k-th component of the vector field associated with system (2).

Computation of $\mathcal{B}$

The coefficient $\mathcal{B}$ involves the mixed second-order partial derivatives $\partial^2 f_k / \partial x_i \partial \beta$ evaluated at $(\mathcal{E}_0, \beta^*)$. The transmission parameter β appears in system (2) only through the new-infection term

$$\beta \left(\mathcal{I}_1 + \eta_1 \mathcal{I}_2 + \eta_2 \mathcal{T} + \eta_3 \mathcal{F} + \eta_4 \mathcal{R} + \eta_5 \mathcal{A} \right) \frac{\mathcal{S}}{\mathcal{N}},$$

in the $\mathcal{I}_1$ equation ($k = 2$). At the disease-free equilibrium the weighted infected sum vanishes, so $\partial^2 f_2/\partial\mathcal{S}\,\partial\beta = 0$, and the only non-zero mixed derivatives are

$$\left.\frac{\partial^2 f_2}{\partial\mathcal{I}_1\,\partial\beta}\right|_{\mathcal{E}_0} = 1, \qquad \left.\frac{\partial^2 f_2}{\partial x_j\,\partial\beta}\right|_{\mathcal{E}_0} = \eta_{j-2}, \quad x_j \in \{\mathcal{I}_2, \mathcal{T}, \mathcal{F}, \mathcal{R}, \mathcal{A}\},$$

where $\eta_0 := 1$ and we have used $\mathcal{S}^0/\mathcal{N}^0 = 1$. Hence

$$\mathcal{B} = v_2\left(w_2 + \eta_1 w_3 + \eta_2 w_4 + \eta_3 w_5 + \eta_4 w_6 + \eta_5 w_7\right).$$

With the standard normalization in which the infected components of the right eigenvector are non-negative ($w_2, \ldots, w_7 \geq 0$, not all zero) and $v_2 > 0$, it follows that $\mathcal{B} > 0$.

Computation of $\mathcal{A}$

The coefficient $\mathcal{A}$ characterizes the second-order nonlinear behaviour of the vector field at $(\mathcal{E}_0, \beta^*)$. The only source of nonlinearity in system (2) is the frequency-dependent incidence term

$$\lambda = \frac{\beta(\cdots)}{\mathcal{N}}.$$

Differentiating $f_2 = \lambda\mathcal{S} - a_1\mathcal{I}_1$ twice with respect to the state variables and evaluating the resulting expressions at $(\mathcal{E}_0, \beta^*)$ yields the second-order contributions computed below.

Because the incidence is frequency dependent, the second-order derivatives of $\lambda\mathcal{S}$ with respect to $\mathcal{S}$ vanish at the disease-free equilibrium,

$$\left.\frac{\partial^2(\lambda\mathcal{S})}{\partial\mathcal{S}\,\partial x_j}\right|_{\mathcal{E}_0} = 0,$$

and the only non-zero contributions arise from pairs of infected variables through the denominator $\mathcal{N}$. Writing $\eta_0 := 1$, a direct computation gives

$$\left.\frac{\partial^2(\lambda\mathcal{S})}{\partial x_i\,\partial x_j}\right|_{\mathcal{E}_0} = -\frac{\beta^*(\eta_{i-2} + \eta_{j-2})}{\mathcal{N}^0}, \qquad x_i, x_j \in \{\mathcal{I}_1, \mathcal{I}_2, \mathcal{T}, \mathcal{F}, \mathcal{R}, \mathcal{A}\},$$

all remaining second derivatives vanishing because the other equations are linear. Substituting into the definition of $\mathcal{A}$ and using $\mathcal{S}^0 = \mathcal{N}^0$ yields the closed form

$$\mathcal{A} = -\frac{2\beta^*}{\mathcal{N}^0}\, v_2 \left(\sum_{j=2}^{7} \eta_{j-2} w_j\right)\left(\sum_{j=2}^{7} w_j\right).$$

Since $v_2 > 0$, $w_j \geq 0$ for $j = 2, \ldots, 7$ (not all zero), and $\eta_{j-2} > 0$, both sums are strictly positive, so $\mathcal{A} < 0$. Hence $\mathcal{A} < 0, \qquad \mathcal{B} > 0$. Therefore, the hypotheses of the centre-manifold theorem of Castillo–Chavez and Song [25] are satisfied, and Theorem 6 follows immediately.

Theorem 6. *Suppose that the centre-manifold coefficients satisfy*

$$\mathcal{A} < 0, \qquad \mathcal{B} > 0.$$

Then, at the threshold $\mathscr{R}_0 = 1$*, system* (2) *undergoes a forward transcritical bifurcation. Furthermore, the bifurcating endemic equilibrium* $\mathcal{E}^*$ *is locally asymptotically stable for values of* $\mathscr{R}_0$ *slightly greater than unity.*

The sign combination $\mathcal{A} < 0$ and $\mathcal{B} > 0$ establishes a forward transcritical bifurcation locally at $\mathscr{R}_0 = 1$; consequently, no backward endemic branch arises in a neighbourhood of the threshold. Thus, near the threshold, reducing $\mathscr{R}_0$ below unity restores the disease-free regime predicted by the local bifurcation analysis.

For values of $\mathscr{R}_0$ sufficiently greater than unity, the local asymptotic stability of the endemic equilibrium $\mathcal{E}^*$ is further verified numerically through direct computation of the eigenvalues of the Jacobian matrix $J(\mathcal{E}^*)$ using the baseline parameter values listed in **Table 1**. For the baseline parameter set, the seven computed eigenvalues are $\{-0.0654,\ -0.00298 \pm 0.00283\,i,\ -0.0188 \pm 0.00910\,i,\ -0.0195,\ -0.0329\}$, all of which lie strictly in the open left half-plane, so the Routh–Hurwitz conditions of Theorem 5 are satisfied for this parameter set and the endemic equilibrium is locally asymptotically stable. We emphasise that this is a numerical verification for the specific baseline values of **Table 1**, not a proof of stability for all $\mathscr{R}_0 > 1$.

Figure 2 provides a numerical illustration consistent with the centre-manifold analysis in Theorem 6. As the effective transmission rate β passes through its critical value β^*, the endemic branch emerges continuously from the disease-free equilibrium, with no backward branch observed over the parameter range examined. This numerical behaviour is consistent with the forward transcritical bifurcation established analytically near $\mathscr{R}_0 = 1$.

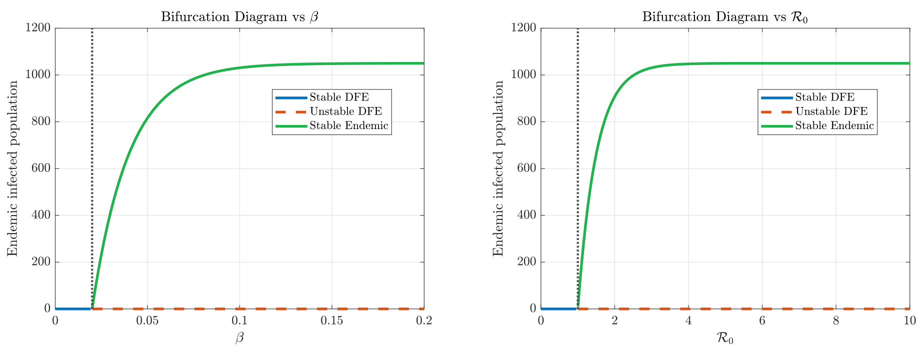

Figure 2. Bifurcation diagram of system (2) with the effective transmission rate β as the bifurcation parameter. For $\mathscr{R}_0 < 1$ (equivalently, $\beta < \beta^*$), the disease-free equilibrium is locally asymptotically stable. As β crosses the critical value β^*, a positive endemic branch emerges continuously from the disease-free equilibrium. Local stability of the bifurcating endemic equilibrium near the threshold follows from the centre-manifold analysis, while stability at the baseline parameter set is verified numerically from the Jacobian eigenvalues. The continuous transition is consistent with a forward transcritical bifurcation and provides no evidence of bistability in the parameter range examined.

Sensitivity analysis

Identifying which parameters carry the most weight in $\mathscr{R}_0$ serves two purposes: it indicates which biological mechanisms the disease is most responsive to, and it guides the choice of control variables in Section 8. We use the normalised forward sensitivity index, defined for a parameter θ as

$$\Upsilon_{\theta}^{\mathscr{R}_0} = \frac{\partial \mathscr{R}_0}{\partial \theta} \frac{\theta}{\mathscr{R}_0},$$

which gives the percentage change in $\mathscr{R}_0$ produced by a one-percent change in θ, and is the standard tool in epidemiological modelling for this purpose [29].

Two of the indices follow immediately from the structure of $\mathscr{R}_0$ in Section 4. Because $\mathscr{R}_0 = \beta P/a_1$ depends linearly on β,

$$\Upsilon_{\beta}^{\mathscr{R}_0} = 1,$$

so a one-percent rise in the transmission rate translates directly into a one-percent rise in $\mathscr{R}_0$. The relative-infectivity modifiers $\eta_1, \ldots, \eta_5$ enter P additively and therefore have uniformly positive indices, the index of η_i being $\eta_i q_{i+1}/P$ (since $\eta_1, \ldots, \eta_5$ multiply $q_2, \ldots, q_6$ in P). The remaining indices were computed by differentiating the closed-form expression for $\mathscr{R}_0$ at the baseline parameter set, taking the midpoint of each range listed in **Table 1** (with Λ excluded because $\mathscr{R}_0$ does not depend on the recruitment rate). The full list of seventeen indices is collected in **Table 2**, sorted by decreasing absolute value, and displayed graphically in **Figure 3**.

Table 2. Normalised forward sensitivity indices of $\mathscr{R}_0$ at the baseline parameter set of **Table 1**, sorted by decreasing absolute value.

Parameter θ	$\Upsilon_{\theta}^{\mathscr{R}_0}$
β	+1.000
η_4	+0.307
δ_3	−0.305
δ_2	−0.277
η_3	+0.230
κ	−0.158
η_5	+0.134
d	−0.133
η_2	+0.091
η_1	+0.064
σ	−0.064
ρ	+0.049
τ	−0.041
δ_1	−0.024
α_2	−0.022
α_1	−0.016
μ	−0.008

A few patterns in **Table 2** are worth pulling out. The transmission rate β dominates the ranking, as expected from its linear appearance in $\mathscr{R}_0$. The next four largest indices, in absolute value, all belong to parameters of the treatment-failure and resistance pathway: η_4 (+0.307), δ_3 (−0.305), δ_2 (−0.277), and η_3 (+0.230). Two readings of this fact are mutually consistent. First, the model is highly responsive to how infectious the late-stage compartments $\mathscr{F}$ and $\mathscr{R}$ are. Second, slow progression from these compartments to AIDS (small δ_2, δ_3) inflates $\mathscr{R}_0$ by extending the time individuals spend transmitting. Together these parameters identify the treatment-failure $\rightarrow$ resistance pathway as the dominant non-acute driver of transmission in the model.

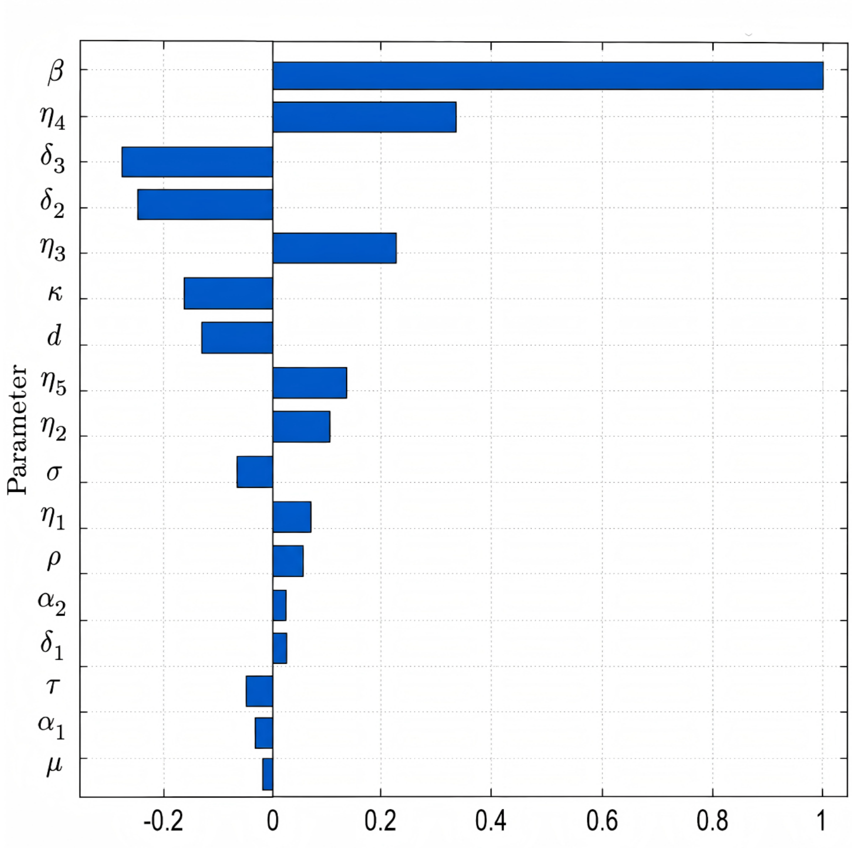

Figure 3. Tornado plot of the normalised sensitivity indices $\Upsilon_{\theta}^{\mathscr{R}_0}$. Bars to the right indicate parameters that increase $\mathscr{R}_0$; bars to the left indicate parameters that decrease it.

The moderate negative sensitivity of the acute-stage progression rate κ indicates that shortening the residence time in the highly infectious acute compartment reduces the overall transmission potential of the disease. The AIDS class is responsible for an additional pair of mid-sized indices, η_5 (+0.13) and d (−0.13), which act in opposite directions through infectivity and mortality, respectively. The treatment uptake rate τ has a modest negative index (−0.04), reflecting the direct effect of ART initiation on shortening the time spent in $\mathscr{I}_2$. Although the remaining parameters exhibit comparatively smaller local sensitivity indices, their cumulative influence along the $\mathscr{T} \rightarrow \mathscr{F} \rightarrow \mathscr{R}$ progression pathway remains epidemiologically important. In particular, the treatment-failure rate σ and the resistance-emergence rate ρ influence the movement of infected individuals through the treatment-failure and drug-resistant compartments. Consequently, even modest changes in these parameters can indirectly alter disease transmission by affecting the duration of infectiousness and the distribution of individuals across the later stages of infection.

These rankings have direct implications for control. Among the biologically actionable parameters, the prevention control u_1 targets β (leverage +1.00), the treatment-uptake control u_2 targets τ (leverage -0.04), and the adherence-support control u_3 targets σ (leverage -0.06). Although the local sensitivity index of σ is negative at the baseline parameter set, this should not be interpreted as implying that treatment failure reduces disease burden. Rather, it reflects the local balance of residence times and infectiousness weights in the closed-form expression for $\mathscr{R}_0$. Biologically, reducing treatment failure remains important because it limits movement into the failure and resistance compartments, whose downstream parameters η_3, η_4, δ_2, and δ_3 have relatively large influence on $\mathscr{R}_0$.

The analytical bifurcation analysis, the numerical bifurcation diagram, and the sensitivity analysis all support a common epidemiological conclusion. The model undergoes a forward transcritical bifurcation at the threshold $\mathscr{R}_0 = 1$, with no evidence of backward bifurcation for the parameter regimes considered. Moreover, the parameters exerting the greatest influence on $\mathscr{R}_0$ correspond directly to the intervention mechanisms incorporated into the optimal control framework developed in the following section, thereby providing a clear analytical justification for the selected control strategies.

7. Numerical results

This section presents numerical simulations of system (2) to provide computational illustrations consistent with the analytical findings, examine the qualitative dynamics of the model, and investigate its response to variations in key epidemiological parameters. We begin by simulating the system (2) using the baseline parameter values listed in **Table 1**, with initial conditions $\mathscr{S}(0) = 1,000$, $\mathscr{I}_1(0) = 10$, $\mathscr{I}_2(0) = 5$, $\mathscr{T}(0) = 0$, $\mathscr{F}(0) = 0$, $\mathscr{R}(0) = 0$, and $\mathscr{A}(0) = 0$.

The system was integrated using MATLAB's variable-step stiff solver `ode15s` with relative and absolute tolerances of 10^{-10} and 10^{-12}, respectively. For the baseline parameter set the basic reproduction number is $\mathscr{R}_0 = 2.57$, and the trajectories converge to the endemic equilibrium $\mathcal{E}^* = (\mathscr{S}^*, \mathscr{I}_1^*, \mathscr{I}_2^*, \mathscr{T}^*, \mathscr{F}^*, \mathscr{R}^*, \mathscr{A}^*) \approx (174.1, 27.8, 15.7, 72.3, 66.7, 57.5, 32.8)$. The disease-free scenario ($\mathscr{R}_0 < 1$) shown below was obtained by reducing the transmission rate to $\beta = 0.006$, with all other parameters unchanged.

Figure 4 illustrates the baseline dynamics of the seven-compartment HIV transmission model in the absence of control interventions. Several features of the trajectories are noteworthy. The susceptible population $\mathscr{S}$ initially remains close to its initial level before gradually declining as the number of infected individuals increases. Following this transient phase, the susceptible population stabilizes at a lower endemic level. The early-infected compartment $\mathscr{I}_1$ increases rapidly during the initial stage of the epidemic, reaches a peak, and then declines as individuals progress from the acute stage to the chronic-infected compartment $\mathscr{I}_2$. In contrast, the chronic-infected compartment increases more gradually before approaching its endemic equilibrium. This behaviour is expected, since progression through the chronic stage occurs over a longer timescale than that of the acute infection.

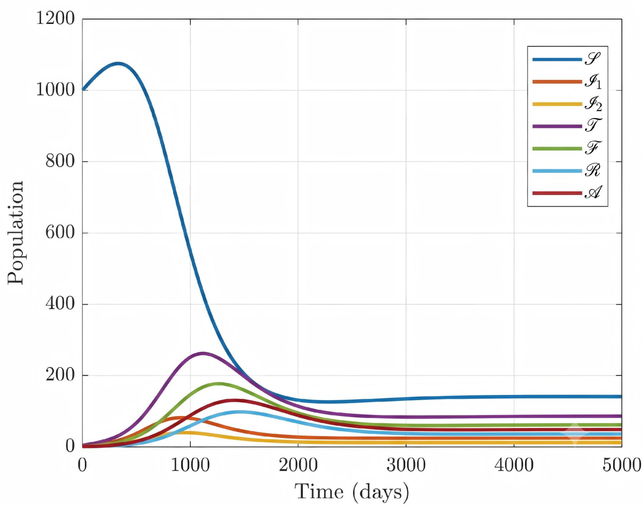

Figure 4. Baseline trajectories of the seven compartments of model (2) over a 5,000-day horizon, starting from a predominantly susceptible population. For the baseline parameter set (**Table 1**, corresponding to $\mathscr{R}_0 > 1$), the susceptible class $\mathscr{S}$ rises to an early peak and then declines as infection spreads, while the six infected compartments $\mathscr{I}_1, \mathscr{I}_2, \mathscr{T}, \mathscr{F}, \mathscr{R}, \mathscr{A}$ grow and subsequently settle at strictly positive steady levels. After an initial transient, the trajectories approach the endemic equilibrium with no sustained oscillations over the simulated horizon. This behaviour is consistent with the parameter-specific stability verification obtained from the eigenvalues of the Jacobian matrix at the endemic equilibrium.

The treated compartment $\mathscr{T}$ also increases before reaching a steady level, indicating that a proportion of infected individuals remain on treatment throughout the simulation period. The treatment-failure compartment $\mathscr{F}$ and the drug-resistant compartment $\mathscr{R}$ emerge more gradually because they are reached only after progression through earlier disease stages. Although their growth is slower, both compartments eventually stabilize at non-negligible levels, indicating that drug-resistant infections continue to contribute to the long-term epidemic dynamics. The AIDS compartment $\mathscr{A}$ likewise increases over time before approaching a positive endemic equilibrium. This behaviour is consistent with the persistent disease-progression pathways included in the uncontrolled model.

These findings predict that all infected compartments converge to strictly positive equilibrium levels rather than declining to zero, confirming the persistence of HIV under the baseline parameter set. This behaviour agrees with Theorem 4, which establishes the existence of a unique endemic equilibrium, and with the local stability criterion of Theorem 5, whose Routh–Hurwitz conditions were verified numerically for this parameter set. The numerical trajectories are therefore consistent with the theoretical analysis and illustrate convergence toward the endemic state for the baseline parameters considered.

7.1. Threshold dynamics

The analytical results of Sections 4 and 5 establish global asymptotic stability of the disease-free equilibrium when $\mathscr{R}_0 < 1$ and the existence of a unique endemic equilibrium when $\mathscr{R}_0 > 1$. Local asymptotic stability of the endemic equilibrium is conditional on the Routh–Hurwitz inequalities stated in Theorem 5. For the baseline parameter set with $\mathscr{R}_0 > 1$, local stability is verified numerically through direct computation of the Jacobian eigenvalues. The simulations should therefore be regarded as parameter-specific numerical evidence supporting the predicted threshold behaviour rather than as a proof of endemic-equilibrium stability for every $\mathscr{R}_0 > 1$.

Figure 5a corresponds to the case $\mathscr{R}_0 < 1$. All infected compartments gradually approach zero, indicating convergence to the disease-free equilibrium. The early-infected compartment $\mathscr{I}_1$ declines rapidly immediately after the start of the simulation, whereas the drug-resistant compartment $\mathscr{R}$ requires a longer time to approach zero. This slower decline is expected because the drug-resistant class is reached only through the treatment-failure pathway and therefore responds more gradually to the reduction in transmission. **Figure 5b** illustrates the opposite case, $\mathscr{R}_0 > 1$. The infected compartments initially increase before converging to positive endemic equilibrium levels. Likewise, the remaining epidemiological compartments approach stable positive steady states, indicating that the disease persists at an endemic level. In particular, the chronic-infected, treated, and drug-resistant compartments attain relatively large equilibrium values under the baseline parameter regime.

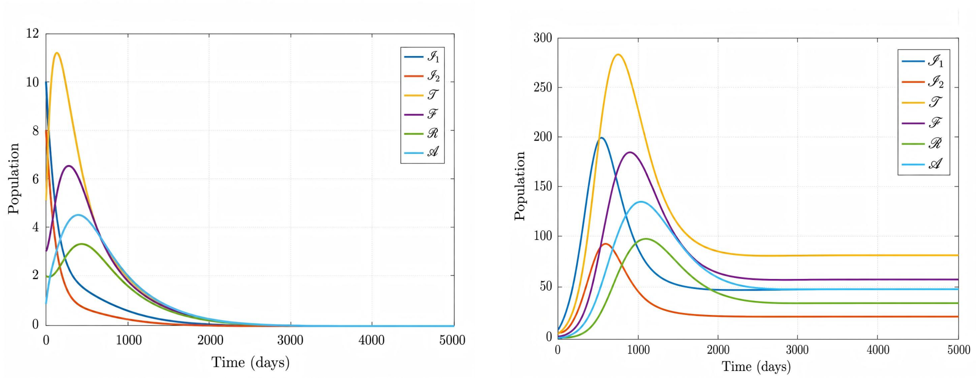

(a) $\mathscr{R}_0 < 1$: decay of all infected compartments and convergence to the disease-free equilibrium.

(b) $\mathscr{R}_0 > 1$: persistence of infection and convergence to the endemic equilibrium.

Figure 5. Threshold behaviour of the six infected compartments $\mathscr{I}_1, \mathscr{I}_2, \mathscr{T}, \mathscr{F}, \mathscr{R}, \mathscr{A}$ over a $5,000$-day horizon for parameter sets on opposite sides of $\mathscr{R}_0 = 1$. When $\mathscr{R}_0 < 1$, the infected compartments decay toward zero, in agreement with the global stability of the disease-free equilibrium. For the parameter set with $\mathscr{R}_0 > 1$, the trajectories approach the corresponding endemic equilibrium. The latter constitutes parameter-specific numerical evidence consistent with the conditional local stability criterion of Theorem 5, rather than a proof of stability for every $\mathscr{R}_0 > 1$.

Another important feature illustrated in **Figure 5** is the continuous transition between the disease-free and endemic regimes as the effective reproduction threshold is crossed. As $\mathscr{R}_0$ approaches unity from above, the endemic equilibrium moves continuously toward the disease-free equilibrium without exhibiting bistability or hysteresis. This numerical behaviour is entirely consistent with the forward transcritical bifurcation established analytically in Theorem 6.

7.2. Effect of epidemiological parameters

To identify the parameters that exert the greatest influence on the disease dynamics, four key epidemiological parameters are varied individually over biologically plausible ranges, while all remaining parameters are maintained at their baseline values. The corresponding responses of the most directly affected infected compartments are presented in **Figure 6**.

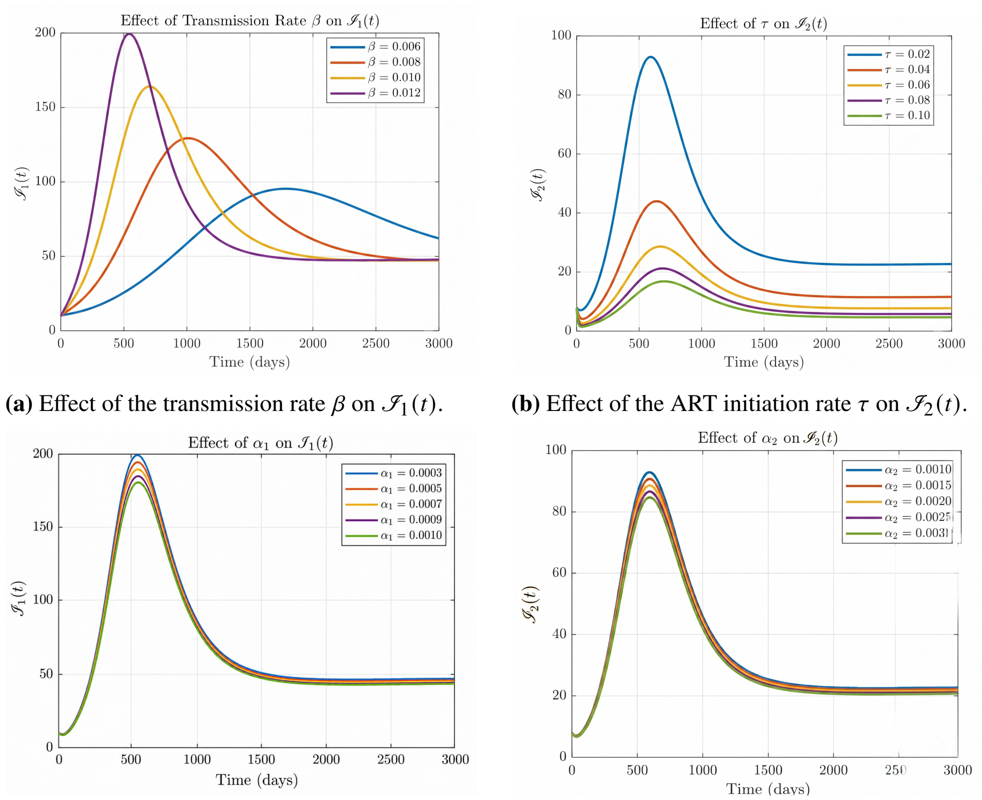

(a) Effect of the transmission rate β on $\mathscr{I}_1(t)$. **(b)** Effect of the ART initiation rate τ on $\mathscr{I}_2(t)$.

(c) Effect of the progression rate α_1 on $\mathscr{I}_1(t)$. **(d)** Effect of the progression rate α_2 on $\mathscr{I}_2(t)$.

Figure 6. Response of the early- and chronic-infected compartments of model (2) to variations in four key epidemiological parameters over a 3,000-day horizon. In each panel a single parameter is swept across five values spanning its range in **Table 1**, while all remaining parameters are held at their baseline values. **(a)** Increasing the effective transmission rate β raises the peak of $\mathscr{I}_1$ and shifts it earlier, confirming β as the dominant driver of infection. **(b)** Increasing the ART initiation rate τ sharply lowers the peak and endemic level of $\mathscr{I}_2$, reflecting the protective effect of earlier treatment. **(c)** Varying the fast-progression rate α_1 and **(d)** the progression rate α_2 produce only small changes in $\mathscr{I}_1$ and $\mathscr{I}_2$, respectively, consistent with the low sensitivity indices of these parameters in **Table 2**.

The transmission rate β, varied in **Figure 6a**, has the most pronounced influence on the model dynamics. Because β enters both the force of infection λ and the expression for $\mathscr{R}_0$ linearly, increasing β substantially raises the equilibrium level of the early-infected compartment $\mathscr{I}_1$ and produces a considerably larger epidemic peak. Although the overall shape of the trajectory remains similar, the magnitude of the outbreak increases noticeably. This observation is consistent with the normalized sensitivity analysis, which identifies β as the parameter with the largest positive sensitivity index. The treatment uptake rate τ, shown in **Figure 6b**, has the opposite effect. Increasing τ from 0.04 to 0.08 accelerates the movement of individuals from the chronic-infected compartment into treatment, thereby reducing the size of $\mathscr{I}_2$. The reduction is not proportional to the increase in τ, however, because the chronic compartment continues to receive new individuals from the acute infection class. Consequently, increasing treatment uptake produces progressively smaller marginal reductions in the chronic-infected population. This observation is consistent with the optimal control analysis presented in Section 8, where treatment expansion forms one component of the combined intervention strategy.

Figure 6c,d illustrates the influence of the progression-to-AIDS rates α_1 and α_2, which appears as additional removal terms in the $\mathscr{I}_1$ and $\mathscr{I}_2$ equations, respectively. Increasing α_1 reduces the size of the early-infected compartment because infected individuals progress more rapidly to the AIDS compartment. The same interpretation applies to α_2 in **Figure 6d**. This reduction should not be interpreted as an improvement in disease control, since infected individuals are not recovering but are instead progressing more rapidly to AIDS. Consequently, the apparent decrease in the infected compartments reflects disease progression rather than successful treatment. From an epidemiological perspective, smaller values of α_i are preferable because they correspond to slower disease progression and a longer period during which infected individuals can benefit from treatment and clinical care.

Taken together, the four panels present a coherent picture of the relative importance of these epidemiological parameters. The model is most sensitive to the transmission rate β, followed by the treatment uptake rate τ, while the effects of α_1 and α_2 require careful epidemiological interpretation. This ordering agrees well with the normalized sensitivity indices presented in Section 6 and further justifies the selection of prevention measures (targeting β) and treatment expansion (targeting τ) as key components of the optimal control strategy developed in Section 8.

7.3. Dependence on initial conditions

Figure 7 illustrates the influence of different initial population distributions on the transient dynamics of $\mathscr{I}_1(t)$ and $\mathscr{I}_2(t)$. For this simulation, all model parameters were fixed at the baseline values of **Table 1**, and the system was integrated over $0 \leq t \leq 3,000$ days using MATLAB's variable-step solver `ode15s` with relative and absolute tolerances 10^{-10} and 10^{-12}, respectively. The four initial conditions, in the component order $(S, \mathscr{I}_1, \mathscr{I}_2, T, F, R, A)$, were $\mathrm{IC}_1 = (4,000, 15, 8, 5, 3, 2, 1)$, $\mathrm{IC}_2 = (4,000, 60, 37, 10, 5, 3, 2)$, $\mathrm{IC}_3 = (4,000, 100, 78, 15, 8, 4, 3)$, and $\mathrm{IC}_4 = (4,000, 140, 90, 20, 10, 5, 4)$. Although the four solutions follow noticeably different trajectories during the early stages of the simulation, these differences progressively diminish. At $t = 3,000$ days, the four simulations yield $\mathscr{I}_1 = 27.901$, 27.882, 27.871, and 27.866, while the corresponding values of $\mathscr{I}_2$ are 15.741, 15.731, 15.725, and 15.722, respectively. These values are close to the baseline endemic-equilibrium components $\mathscr{I}_1^* \approx 27.8$ and $\mathscr{I}_2^* \approx 15.7$. Thus, for these four initial states and the baseline parameter set, the simulations provide parameter-specific numerical evidence of attraction toward the same endemic equilibrium. This observation is consistent with the local stability analysis but should not be interpreted as a proof of global asymptotic stability.

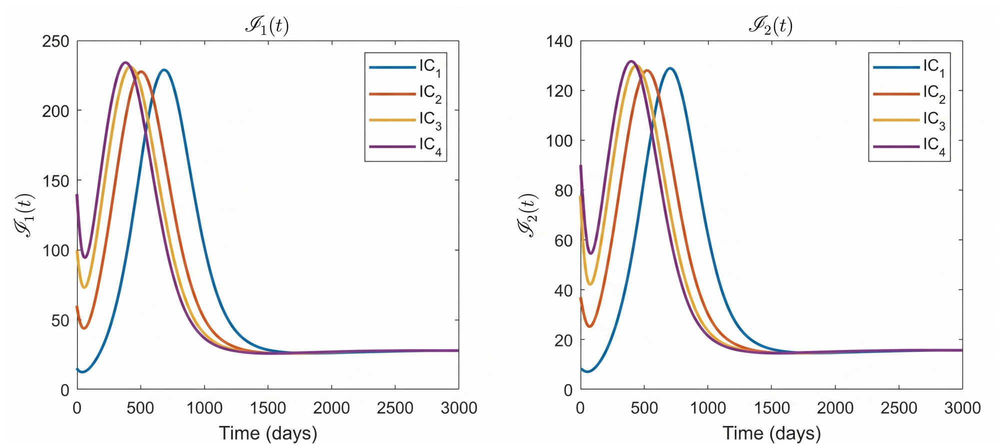

Figure 7. Dependence of the early- and chronic-infected compartments $\mathscr{I}_1(t)$ and $\mathscr{I}_2(t)$ on four distinct initial conditions over a 3,000-day simulation horizon, with all model parameters fixed at the baseline values of **Table 1**. The four initial states, in the component order $(S, \mathscr{I}_1, \mathscr{I}_2, T, F, R, A)$, are $\text{IC}_1 = (4,000, 15, 8, 5, 3, 2, 1)$, $\text{IC}_2 = (4,000, 60, 37, 10, 5, 3, 2)$, $\text{IC}_3 = (4,000, 100, 78, 15, 8, 4, 3)$, and $\text{IC}_4 = (4,000, 140, 90, 20, 10, 5, 4)$. Despite different transient responses, the trajectories approach essentially the same endemic state for the baseline parameter set.

7.4. Phase-plane analysis

To further examine the qualitative dynamics of the model, **Figure 8** presents three phase-plane projections of the trajectory obtained for the baseline parameter set. The displayed projections exhibit a strongly damped oscillatory approach toward the endemic equilibrium, consistent with the complex-conjugate eigenvalue pairs having negative real parts together with the remaining negative real eigenvalues reported in Section 5. Although no closed curve is observed over the simulated trajectory, these two-dimensional projections do not constitute a proof that periodic solutions are absent from the full seven-dimensional system.

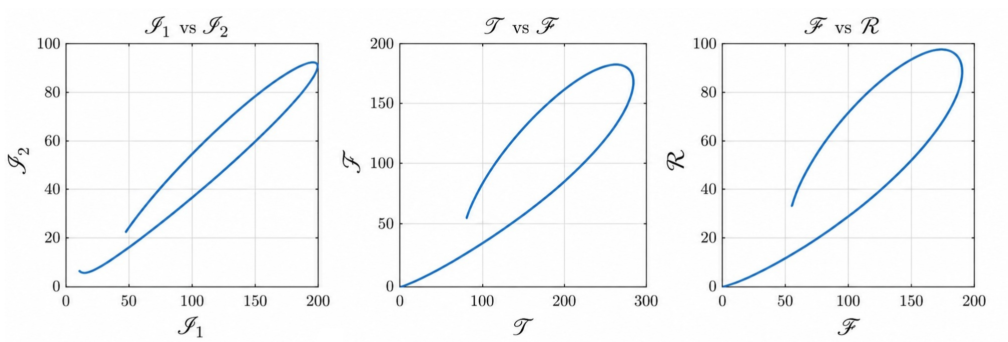

Figure 8. Phase-plane projections of the state trajectory of model (2) onto three pairs of compartments: the early- versus chronic-infected classes ($\mathscr{I}_1$ vs. $\mathscr{I}_2$), the treated versus treatment-failure classes ($\mathscr{T}$ vs. $\mathscr{F}$), and the treatment-failure versus drug-resistant classes ($\mathscr{F}$ vs. $\mathscr{R}$), for the baseline parameter set of **Table 1**, for which $\mathscr{R}_0 > 1$. In each projection, the displayed orbit approaches an interior endemic equilibrium through a strongly damped oscillatory transient. This behaviour is consistent with the complex-conjugate eigenvalue pairs having negative real parts, together with the remaining negative real eigenvalues reported in Section 5. None of the displayed projections form a closed curve over the simulated trajectory. However, a two-dimensional projection of a seven-dimensional system cannot by itself establish the absence of periodic orbits in the full system.

7.5. Sensitivity heatmap

To complement the normalized sensitivity analysis presented in Section 6, **Figure 9** illustrates the joint dependence of the basic reproduction number on the effective transmission rate β together with two intervention-related parameters: the treatment-failure rate σ and the treatment uptake rate τ. These graphical results provide additional insight into how simultaneous changes in key epidemiological parameters influence the disease transmission threshold.

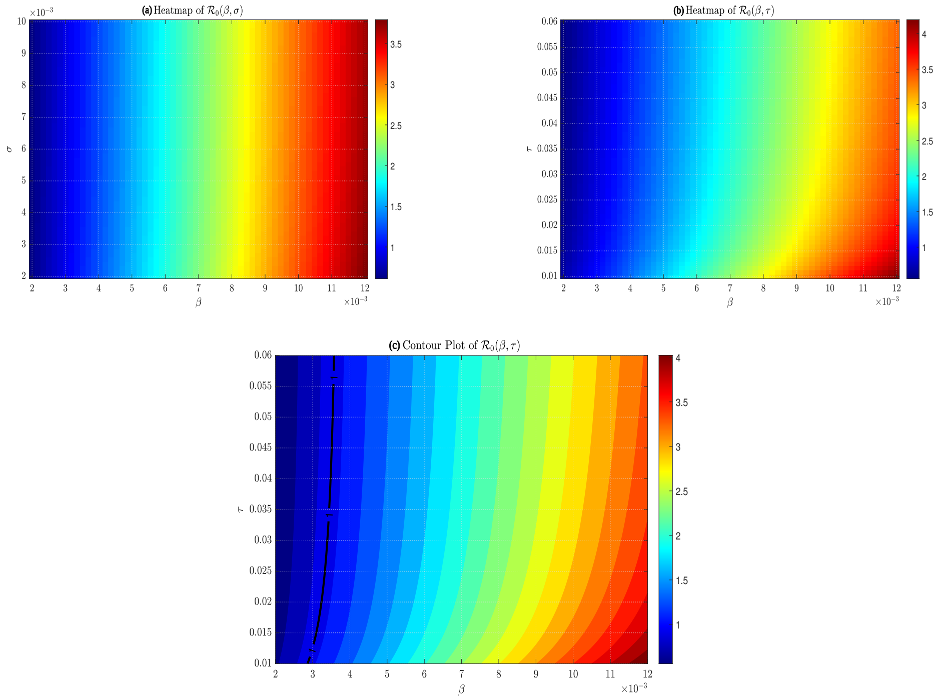

Figure 9. Joint dependence of the basic reproduction number $\mathscr{R}_0$ of model (2) on the effective transmission rate β and two control-relevant parameters, the treatment-failure rate σ and the ART uptake rate τ, with all remaining parameters fixed at the baseline values of **Table 1**. **(a)** heatmap of $\mathscr{R}_0(\beta,\sigma)$, showing that $\mathscr{R}_0$ increases sharply with β but is almost insensitive to σ, so the level curves are nearly vertical. **(b)** heatmap of $\mathscr{R}_0(\beta,\tau)$, showing that raising τ lowers $\mathscr{R}_0$ and bends the contours, so increased treatment uptake partially offsets a higher transmission rate. **(c)** contour plot of $\mathscr{R}_0(\beta,\tau)$ with the critical threshold $\mathscr{R}_0 = 1$ marked in black; this curve separates the disease-free region ($\mathscr{R}_0 < 1$, left) from the endemic region ($\mathscr{R}_0 > 1$, right). Together the panels confirm β as the dominant driver of $\mathscr{R}_0$ and τ as the more effective control lever, in agreement with the sensitivity ranking in **Table 2**.

Across the parameter ranges examined, the effective transmission rate β emerges as the parameter with the greatest impact on $\mathscr{R}_0$. As β increases, the basic reproduction number rises rapidly, whereas comparatively smaller changes are observed when either σ or τ is varied over their respective ranges. These observations are consistent with the normalized sensitivity analysis, which identified β as the most influential parameter governing HIV transmission. From a public-health perspective, this highlights the importance of interventions that reduce transmission, such as behavioural modification, condom use, and other preventive measures.

The heatmap of $\mathscr{R}_0(\beta,\sigma)$ further shows that the basic reproduction number is considerably more sensitive to changes in β than to variations in the treatment-failure rate σ. Under the baseline parameter regime considered in this study, increasing σ

produces only a modest reduction in $\mathscr{R}_0$, consistent with the analytical sensitivity results. This behaviour is consistent with the combined influence of the transition pathways represented in the model and indicates that the overall effect of σ on the transmission threshold is relatively small compared with that of the transmission rate itself.

Similarly, the heatmap and contour plot of $\mathscr{R}_0(\beta, \tau)$ demonstrate that increasing the treatment uptake rate τ reduces the basic reproduction number, although its effect remains less pronounced than that of β. The contour plot clearly identifies the combinations of β and τ for which $\mathscr{R}_0 < 1$, thereby illustrating the threshold required for disease elimination under the assumptions of the model. The nearly vertical contour lines indicate that reducing the transmission rate produces a substantially larger impact on $\mathscr{R}_0$ than comparable changes in treatment uptake alone. The results presented in **Figure 9** reinforce the analytical sensitivity results and demonstrate that reducing the effective transmission rate remains the most influential strategy for lowering the basic reproduction number. At the same time, increasing treatment uptake and improving treatment outcomes provide valuable complementary benefits by further reducing the transmission potential and supporting long-term HIV control.

7.6. Summary of numerical findings

The numerical simulations presented in this section are consistent with the analytical threshold results and provide parameter-specific evidence for attraction toward the endemic equilibrium when $\mathscr{R}_0 > 1$. They also illustrate the influence of key epidemiological parameters on the qualitative dynamics of the model. These computations should not be interpreted as a proof of global attraction or as calibrated predictions for a particular population. The numerical experiments further identify the effective transmission rate as an important driver of disease persistence, while treatment uptake, treatment failure, and resistance-related parameters influence the distribution of individuals among the infected compartments. These findings are consistent with the normalized sensitivity analysis and motivate the intervention mechanisms incorporated into the optimal control framework developed in the next section.

8. Optimal control analysis

To investigate the combined impact of prevention, treatment initiation, and adherence support, we introduce three time-dependent control functions representing feasible public-health interventions. The control $u_1(t) \in [0, 1]$ represents preventive effort and reduces the effective transmission rate from β to $(1 - u_1)\beta$. This control aggregates condom-promotion campaigns, pre-exposure prophylaxis coverage, and behavioural interventions into a single dimensionless measure.

The control $u_2(t) \in [0, 1]$ represents enhanced treatment uptake and increases the ART initiation rate from τ to $\tau(1+u_2)$, thereby modelling expanded access to ART. The control $u_3(t) \in [0, 1]$ represents adherence-strengthening interventions and reduces the treatment-failure rate from σ to $\sigma(1-u_3)$. Such interventions may include counselling, peer-support programmes, and electronic adherence monitoring. Here, λ denotes the baseline force of infection defined in Equation (3); under the prevention control, the effective force of infection becomes $(1 - u_1)\lambda$.

Substituting the three controls into system (2) yields the controlled system

$$\begin{cases} \dot{\mathcal{S}} = \Lambda - (1 - u_1)\lambda\mathcal{S} - \mu\mathcal{S}, \\ \dot{\mathcal{I}}_1 = (1 - u_1)\lambda\mathcal{S} - (\kappa + \mu + \alpha_1)\mathcal{I}_1, \\ \dot{\mathcal{I}}_2 = \kappa\mathcal{I}_1 - \big(\tau(1 + u_2) + \mu + \alpha_2\big)\mathcal{I}_2, \\ \dot{\mathcal{T}} = \tau(1 + u_2)\mathcal{I}_2 - \big(\sigma(1 - u_3) + \mu + \delta_1\big)\mathcal{T}, \\ \dot{\mathcal{F}} = \sigma(1 - u_3)\mathcal{T} - (\rho + \mu + \delta_2)\mathcal{F}, \\ \dot{\mathcal{R}} = \rho\mathcal{F} - (\mu + \delta_3)\mathcal{R}, \\ \dot{\mathcal{A}} = \alpha_1\mathcal{I}_1 + \alpha_2\mathcal{I}_2 + \delta_1\mathcal{T} + \delta_2\mathcal{F} + \delta_3\mathcal{R} - (\mu + d)\mathcal{A}. \end{cases} \tag{24}$$

The force of infection is

$$\lambda = \frac{\beta\left(\mathcal{I}_1 + \eta_1\mathcal{I}_2 + \eta_2\mathcal{T} + \eta_3\mathcal{F} + \eta_4\mathcal{R} + \eta_5\mathcal{A}\right)}{\mathcal{N}},$$

and the control set is defined by

$$\mathcal{U} = \left\{(u_1, u_2, u_3) \in \left(L^\infty(0, T)\right)^3 : 0 \leq u_i(t) \leq 1 \text{ for a.e. } t \in [0, T],\ i = 1, 2, 3\right\}.$$

The objective is to minimize the cumulative epidemiological burden over a fixed planning horizon while simultaneously accounting for the costs associated with implementing the control measures. We therefore define the quadratic cost functional

$$\begin{aligned} &\mathcal{J}(u_1, u_2, u_3) \\ &= \int_0^T \left[C_1\mathcal{I}_1 + C_2\mathcal{I}_2 + C_3\mathcal{F} + C_4\mathcal{R} + C_5\mathcal{A} + \frac{1}{2}\left(D_1u_1^2 + D_2u_2^2 + D_3u_3^2\right)\right] dt. \end{aligned} \tag{25}$$

The positive weights $C_1, \ldots, C_5$ quantify the per-capita burden associated with the corresponding infected compartments, whereas $D_1, D_2, D_3 > 0$ represent the implementation costs of applying each control at unit intensity. A quadratic control cost is standard in epidemiological optimal control models and reflects the increasing marginal cost associated with higher intervention intensity. The numerical values of the state and control weights used in all optimal-control simulations are listed in **Table 3**.

Table 3. State and control weight coefficients used in the objective functional Equation (25) for the optimal-control simulations.

Coefficient	Description	Value
C_1	Burden weight, early-infected $\mathcal{I}_1$	1
C_2	Burden weight, chronic-infected $\mathcal{I}_2$	1
C_3	Burden weight, treatment-failure $\mathcal{F}$	5
C_4	Burden weight, drug-resistant $\mathcal{R}$	5
C_5	Burden weight, AIDS class $\mathcal{A}$	10
D_1	Cost weight, prevention control u_1	50
D_2	Cost weight, treatment-uptake control u_2	8
D_3	Cost weight, adherence-support control u_3	20

The treated compartment $\mathscr{T}$ is not included in the state cost because individuals receiving successful suppressive therapy represent a desirable treatment outcome rather than an epidemiological burden targeted for reduction. Penalizing $\mathscr{T}$ would therefore introduce an unintended disincentive against the treatment uptake control u_2. The optimal control problem is to determine $(u_1^*, u_2^*, u_3^*) \in \mathcal{U}$ such that

$$\mathcal{J}(u_1^*, u_2^*, u_3^*) = \inf_{(u_1,u_2,u_3)\in\mathcal{U}} \mathcal{J}(u_1, u_2, u_3),$$

subject to the controlled state system (24) and biologically admissible initial conditions.

8.1. Existence of an optimal control

Before characterizing the optimal controls, we establish the existence of at least one minimizing control triple using the classical existence framework of Fleming–Rishel [40].

Theorem 7. *The optimal control problem admits at least one admissible control triple*

$$(u_1^*, u_2^*, u_3^*) \in \mathcal{U}$$

for which the objective functional $\mathcal{J}$ in Equation (25) *attains its minimum, under the dynamics prescribed by the controlled system* (24).

Proof. We verify the standard conditions required for the existence of an optimal control.

(i) Existence of admissible state–control pairs. The admissible control class $\mathcal{U}$ is non-empty, since the identically zero control

$$(u_1, u_2, u_3) \equiv (0, 0, 0)$$

is an element of $\mathcal{U}$. For any control chosen from this set, the vector field associated with system (24) is measurable with respect to time, continuous in the control variables, and locally Lipschitz in the state variables. Consequently, the Carathéodory existence theory applies, ensuring the existence of a unique local solution that is absolutely continuous.

Summing the equations of the controlled system gives

$$\frac{d\mathscr{N}}{dt} = \Lambda - \mu\mathscr{N} - d\mathscr{A} \leq \Lambda - \mu\mathscr{N}.$$

Therefore, the positivity and boundedness arguments established in Theorem 1 remain valid for every admissible control. In particular, the controlled solution exists on the entire interval $[0, T]$, and the set of admissible state-control pairs is non-empty.

(ii) Properties of the admissible control set. The set $\mathcal{U}$ is non-empty, closed, convex, and bounded in $\left(L^\infty(0,T)\right)^3$. The pointwise control set $[0, 1]^3$ is compact and convex, and the admissible controls satisfy the required measurability and boundedness conditions.

(iii) Affine dependence on the controls and linear growth of the state system. For a fixed state, the right-hand side of system (24) depends affinely on (u_1, u_2, u_3). Moreover, the population bound established above implies that all state variables remain bounded. Consequently, there exist constants $K_1, K_2 \geq 0$ such that

$$\|f(x, u, t)\| \leq K_1 + K_2\|x\|, \qquad \text{uniformly for } u \in \mathcal{U}.$$

(iv) Convexity and coercivity of the integrand. The running cost

$$\mathcal{L}(x, u) = C_1\mathscr{I}_1 + C_2\mathscr{I}_2 + C_3\mathscr{F} + C_4\mathscr{R} + C_5\mathscr{A} + \frac{1}{2}\left(D_1u_1^2 + D_2u_2^2 + D_3u_3^2\right)$$

is affine in the state variables and strictly convex in the controls because $D_i > 0$ for $i = 1, 2, 3$. Since the state variables and the weights C_i are non-negative,

$$\mathcal{L}(x, u) \geq \frac{1}{2}\min\{D_1, D_2, D_3\}\,\|u\|^2.$$

Thus, the integrand satisfies the required coercivity condition.

All the requirements of the Fleming–Rishel existence theorem are thus fulfilled. Consequently, the optimal control problem admits at least one solution

$$(u_1^*, u_2^*, u_3^*) \in \mathcal{U}.$$

□

8.2. Characterization of the optimal controls

The necessary conditions for optimality are derived using Pontryagin's Maximum Principle [30,31], which provides first-order necessary conditions for an optimal control and its corresponding state trajectory. To avoid a notational conflict between the force of infection λ and the adjoint variables, we denote the latter by $\psi_1, \ldots, \psi_7$.

Let

$$x = (\mathscr{S}, \mathscr{I}_1, \mathscr{I}_2, \mathscr{T}, \mathscr{F}, \mathscr{R}, \mathscr{A}),$$

denote the state vector, while $f = (f_1, \ldots, f_7)$ denotes the vector field corresponding to the right-hand side of the controlled system (24). By applying Pontryagin's Maximum Principle, the necessary optimality conditions are formulated in terms of the state system, the corresponding adjoint system, and the condition minimizing the Hamiltonian. We therefore introduce the Hamiltonian for the control problem before deriving these necessary conditions. The Hamiltonian is given by

$$\begin{aligned}\mathcal{H} &= C_1\mathscr{I}_1 + C_2\mathscr{I}_2 + C_3\mathscr{F} + C_4\mathscr{R} + C_5\mathscr{A} \\ &\quad + \frac{1}{2}\left(D_1u_1^2 + D_2u_2^2 + D_3u_3^2\right) + \sum_{i=1}^{7}\psi_i f_i.\end{aligned} \tag{26}$$

Theorem 8 (Pontryagin characterization)**.** *Let (u_1^*, u_2^*, u_3^*) be an optimal control triple, and let*

$$x^* = (\mathscr{S}^*, \mathscr{I}_1^*, \mathscr{I}_2^*, \mathscr{T}^*, \mathscr{F}^*, \mathscr{R}^*, \mathscr{A}^*),$$

be the corresponding optimal state trajectory. Then there exists an adjoint vector

$$\psi(t) = (\psi_1(t), \ldots, \psi_7(t)),$$

satisfying

$$\dot{\psi}_i(t) = -\frac{\partial \mathcal{H}}{\partial x_i}\bigg|_{x^*,u^*}, \qquad \psi_i(T) = 0, \qquad i = 1, \ldots, 7.$$

Moreover, for almost every $t \in [0, T]$, the optimal control (u_1^*, u_2^*, u_3^*) minimizes the Hamiltonian over the admissible control set $[0, 1]^3$ and is characterized by

$$u_1^* = \min\left\{1, \max\left[0, \frac{(\psi_2 - \psi_1)\lambda^* \mathcal{S}^*}{D_1}\right]\right\}, \tag{27}$$

$$u_2^* = \min\left\{1, \max\left[0, \frac{\tau \mathcal{I}_2^*(\psi_3 - \psi_4)}{D_2}\right]\right\}, \tag{28}$$

$$u_3^* = \min\left\{1, \max\left[0, \frac{\sigma \mathcal{T}^*(\psi_5 - \psi_4)}{D_3}\right]\right\}. \tag{29}$$

Here, λ^* denotes the force of infection evaluated along the optimal state trajectory.

Proof. The existence of the adjoint variables and the transversality conditions

$$\psi_i(T) = 0, \qquad i = 1, \ldots, 7,$$

as a consequence of Pontryagin's Maximum Principle [30]. To obtain explicit expressions for the optimal controls, the Hamiltonian is differentiated with respect to the corresponding control variables, after which the pointwise minimization requirement is imposed over the admissible control set. In particular, for the control u_1, the terms of the Hamiltonian that depend explicitly on u_1 are

$$\frac{1}{2}D_1 u_1^2 + \psi_1 u_1 \lambda \mathcal{S} - \psi_2 u_1 \lambda \mathcal{S}.$$

Hence,

$$\frac{\partial \mathcal{H}}{\partial u_1} = D_1 u_1 + \lambda \mathcal{S}(\psi_1 - \psi_2).$$

Similarly,

$$\frac{\partial \mathcal{H}}{\partial u_2} = D_2 u_2 + \tau \mathcal{I}_2(\psi_4 - \psi_3),$$

and

$$\frac{\partial \mathcal{H}}{\partial u_3} = D_3 u_3 + \sigma \mathcal{T}(\psi_4 - \psi_5).$$

Equating these partial derivatives to zero gives the corresponding unconstrained expressions for the control variables

$$\widetilde{u}_1 = \frac{(\psi_2 - \psi_1)\lambda \mathcal{S}}{D_1}, \qquad \widetilde{u}_2 = \frac{\tau \mathcal{I}_2(\psi_3 - \psi_4)}{D_2}, \qquad \widetilde{u}_3 = \frac{\sigma \mathcal{T}(\psi_5 - \psi_4)}{D_3}.$$

Projecting these expressions onto the admissible interval $[0, 1]$ gives the control characterizations (27)–(29). □

The adjoint equations are obtained from

$$\dot{\psi}_i = -\frac{\partial \mathcal{H}}{\partial x_i}, \qquad i = 1, \ldots, 7,$$

explicitly,

$$\dot{\psi}_1 = \mu\psi_1 + (1 - u_1)\left(\lambda + \mathcal{S}\frac{\partial\lambda}{\partial\mathcal{S}}\right)(\psi_1 - \psi_2), \tag{30}$$

$$\begin{aligned}\dot{\psi}_2 = & -C_1 + (\kappa + \mu + \alpha_1)\psi_2 - \kappa\psi_3 - \alpha_1\psi_7 \\ & + (1 - u_1)\mathcal{S}\frac{\partial\lambda}{\partial\mathcal{I}_1}(\psi_1 - \psi_2),\end{aligned} \tag{31}$$

$$\begin{aligned}\dot{\psi}_3 = & -C_2 + \big(\tau(1 + u_2) + \mu + \alpha_2\big)\psi_3 - \tau(1 + u_2)\psi_4 - \alpha_2\psi_7 \\ & + (1 - u_1)\mathcal{S}\frac{\partial\lambda}{\partial\mathcal{I}_2}(\psi_1 - \psi_2),\end{aligned} \tag{32}$$

$$\begin{aligned}\dot{\psi}_4 = & \big(\sigma(1 - u_3) + \mu + \delta_1\big)\psi_4 - \sigma(1 - u_3)\psi_5 - \delta_1\psi_7 \\ & + (1 - u_1)\mathcal{S}\frac{\partial\lambda}{\partial\mathcal{T}}(\psi_1 - \psi_2),\end{aligned} \tag{33}$$

$$\begin{aligned}\dot{\psi}_5 = & -C_3 + (\rho + \mu + \delta_2)\psi_5 - \rho\psi_6 - \delta_2\psi_7 \\ & + (1 - u_1)\mathcal{S}\frac{\partial\lambda}{\partial\mathcal{F}}(\psi_1 - \psi_2),\end{aligned} \tag{34}$$

$$\begin{aligned}\dot{\psi}_6 = & -C_4 + (\mu + \delta_3)\psi_6 - \delta_3\psi_7 \\ & + (1 - u_1)\mathcal{S}\frac{\partial\lambda}{\partial\mathcal{R}}(\psi_1 - \psi_2),\end{aligned} \tag{35}$$

$$\dot{\psi}_7 = -C_5 + (\mu + d)\psi_7 + (1 - u_1)\mathcal{S}\frac{\partial\lambda}{\partial\mathcal{A}}(\psi_1 - \psi_2), \tag{36}$$

subject to the transversality conditions

$$\psi_i(T) = 0, \qquad i = 1, \ldots, 7. \tag{37}$$

Differentiating the standard-incidence force of infection

$$\lambda = \frac{\beta\left(\mathcal{I}_1 + \eta_1\mathcal{I}_2 + \eta_2\mathcal{T} + \eta_3\mathcal{F} + \eta_4\mathcal{R} + \eta_5\mathcal{A}\right)}{\mathcal{N}}$$

with respect to the state variables gives

$$\frac{\partial\lambda}{\partial\mathcal{S}} = -\frac{\lambda}{\mathcal{N}}, \qquad \frac{\partial\lambda}{\partial\mathcal{I}_1} = \frac{\beta - \lambda}{\mathcal{N}}, \qquad \frac{\partial\lambda}{\partial\mathcal{I}_2} = \frac{\beta\eta_1 - \lambda}{\mathcal{N}},$$

$$\frac{\partial\lambda}{\partial\mathcal{T}} = \frac{\beta\eta_2 - \lambda}{\mathcal{N}}, \qquad \frac{\partial\lambda}{\partial\mathcal{F}} = \frac{\beta\eta_3 - \lambda}{\mathcal{N}}, \qquad \frac{\partial\lambda}{\partial\mathcal{R}} = \frac{\beta\eta_4 - \lambda}{\mathcal{N}},$$

and

$$\frac{\partial\lambda}{\partial\mathcal{A}} = \frac{\beta\eta_5 - \lambda}{\mathcal{N}}.$$

The complete optimality system consists of the controlled state Equation (24), the adjoint Equations (30)–(36), the transversality conditions (37), and the control characterizations (27)–(29). This coupled system is solved numerically using the forward–backward sweep algorithm.

8.3. Numerical solution of the optimality system

To compute the optimality system numerically, we employ the forward–backward sweep method. The procedure starts with an initial approximation of the control functions. Using these controls, the state system (24) is solved forward over the interval $[0, T]$ from the prescribed initial data. The resulting state trajectories are then used to solve the adjoint systems (30)–(36) backward in time, beginning at $t = T$ and satisfying the terminal conditions in Equation (37).

Once the state and adjoint variables have been obtained, new control profiles are computed from the optimal-control expressions stated in Theorem 8. These updated controls are subsequently used in the next forward integration of the state system. Because the state, costate, and control variables depend on one another, this forward–backward process is carried out repeatedly rather than in a single pass. The iterations are terminated when the changes in the state, adjoint, and control approximations between two consecutive iterations are smaller than a prescribed tolerance [31].

For all optimal-control simulations, the forward–backward sweep was implemented on a uniform time grid over the horizon $T = 300$ days with $2,000$ subintervals. The state and adjoint systems were integrated by a fourth-order Runge–Kutta scheme, and the sweep was iterated with a relaxation factor of 0.5 until the relative change in successive control iterates fell below 10^{-4}. The initial conditions were $(\mathcal{S}, \mathcal{I}_1, \mathcal{I}_2, \mathcal{T}, \mathcal{F}, \mathcal{R}, \mathcal{A})(0) = (2.0 \times 10^4, 50, 30, 10, 5, 2, 2)$, all model parameters were fixed at the baseline values of **Table 1**, and the objective weights were set as listed in **Table 3**.

Figure 10 compares the epidemic dynamics generated by the uncontrolled model with those obtained under the optimal three-control strategy. Simultaneous implementation of the prevention, treatment-initiation, and adherence-support controls substantially reduces the total infectious burden throughout the intervention horizon. Although the infection is not eradicated within the finite simulation period, the controlled solution consistently remains well below the uncontrolled trajectory, demonstrating the effectiveness of the combined intervention strategy. A substantial reduction in the total infected population is observed throughout the intervention horizon when the three controls are implemented simultaneously. Although the epidemic is not eliminated within the finite simulation period, the combined strategy consistently suppresses disease transmission and produces a markedly lower infectious burden than the uncontrolled scenario. This demonstrates the complementary nature of prevention, treatment initiation, and adherence support, whose simultaneous implementation provides a considerably greater epidemiological benefit than allowing the epidemic to evolve without intervention.

The optimal control trajectories obtained from the analysis are displayed in **Figure 11**. In particular, the prevention strategy $u_1^*(t)$ remains relatively intensive at the beginning of the control period, indicating that early preventive efforts play a key role in limiting the emergence and subsequent spread of new HIV infections. Its gradual relaxation towards the terminal time is consistent with the finite planning horizon and the transversality conditions $\psi_i(T) = 0$, under which the marginal benefit of preventing future infections decreases as the terminal time is approached. The treatment initiation control $u_2^*(t)$ remains active throughout the intervention period, although at a lower intensity, indicating that continuous expansion of ART uptake contributes to limiting disease progression. In contrast, the adherence-support control $u_3^*(t)$ remains close to its upper bound over most of the simulation horizon, suggesting that sustained adherence interventions are a highly effective mechanism for reducing downstream disease progression. As above, this conclusion is specific to the state and control weights adopted here and to the form of the objective functional, and no economic cost-effectiveness analysis is implied.

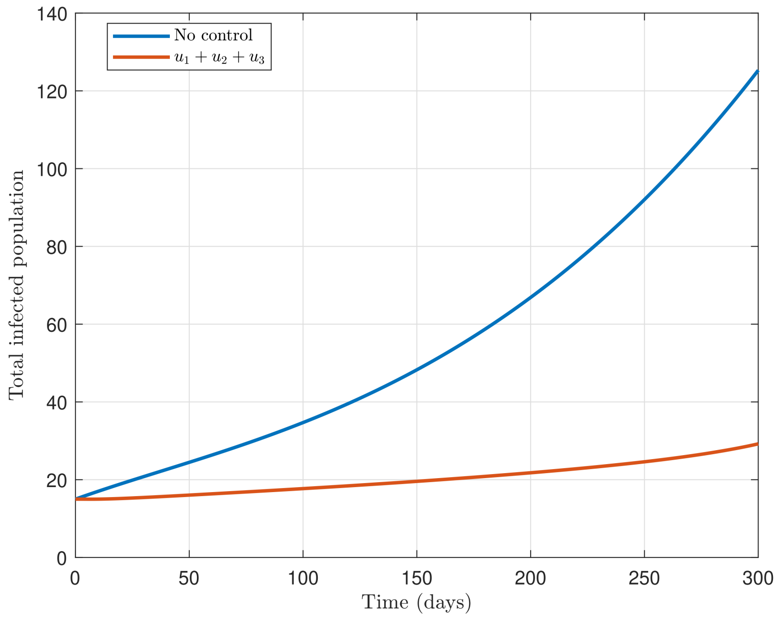

Figure 10. Comparison of the total infected population under the uncontrolled scenario and the optimal three-control strategy (u_1, u_2, u_3). The simultaneous implementation of prevention, treatment initiation, and adherence support substantially reduces the infectious burden throughout the intervention horizon. Although the epidemic is not eliminated within the finite time interval considered, the combined strategy consistently suppresses disease transmission relative to the uncontrolled case, demonstrating the overall effectiveness of the proposed optimal intervention framework.

The robustness calculations shown in **Figures 12** and **13** examine independent $\pm 20\%$ perturbations of the control-cost coefficients around the baseline weighting scheme. Within this tested range, the controlled trajectories and cumulative infected burden change only modestly, while the main qualitative behaviour of the optimized three-control strategy is preserved. These numerical results therefore suggest local robustness with respect to moderate perturbations of the chosen control-cost coefficients.

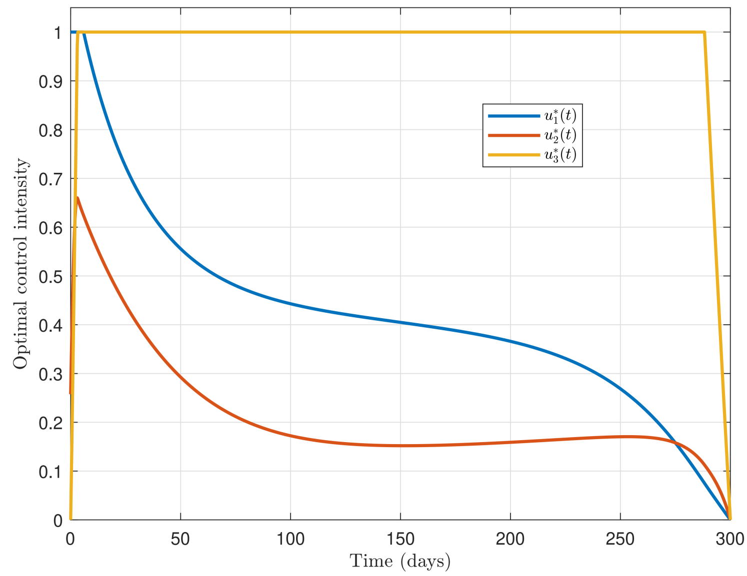

Figure 11. Optimal time-dependent control profiles obtained using the forward–backward sweep algorithm. The prevention control $u_1^*(t)$ is initially implemented at a high intensity and is gradually relaxed as the infectious burden decreases. The treatment initiation control $u_2^*(t)$ follows a moderate intervention schedule, whereas the adherence-support control $u_3^*(t)$ remains close to its upper bound for most of the intervention period. This suggests that sustained adherence support is a highly effective component of the control strategy for limiting treatment failure and the emergence of drug resistance. We stress that this conclusion is specific to the state and control weights adopted here (**Table 3**) and to the form of the objective functional; different weightings may alter the relative prominence of the individual controls.

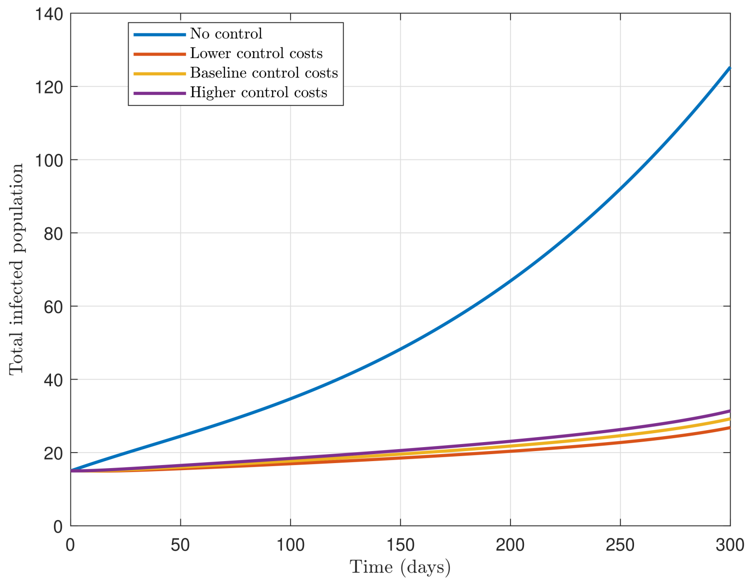

Figure 12. Robustness analysis of the optimal three-control strategy under ±20% perturbations of the control-cost coefficients. Within the tested range, the controlled trajectories retain qualitatively similar behaviour. These computations provide local numerical evidence of robustness around the baseline weighting scheme and do not imply insensitivity to arbitrary choices of the objective-function weights.

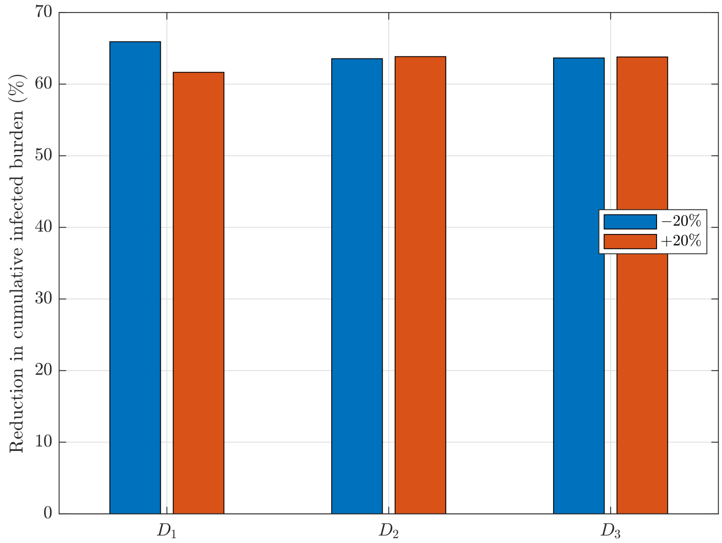

Figure 13. Sensitivity of the cumulative infected burden to independent ±20% variations in the control-cost coefficients D_1, D_2, and D_3. The relatively modest changes observed within this range provide local numerical evidence of robustness around the baseline weighting scheme. Substantially different weighting choices may lead to different optimal control profiles and intervention rankings.

This finding should not be interpreted as independence from the weighting parameters in general. Substantially different state or control weights may alter the optimal control profiles and the relative prominence of the three intervention mechanisms. Accordingly, the present results establish robustness only within the range of weight perturbations examined numerically.

9. Conclusion

In this study, we developed and analyzed a nonlinear seven-compartment HIV transmission model that incorporates stage-wise disease progression, ART uptake, adherence-mediated treatment failure, and acquired drug resistance. The proposed model was shown to be mathematically well-posed through the establishment of positivity, boundedness, and the existence of a biologically feasible invariant region. The basic reproduction number, $\mathscr{R}_0$, derived using the next-generation matrix approach, serves as the principal threshold parameter governing the disease dynamics. The disease-free equilibrium was shown to be locally and globally asymptotically stable for $\mathscr{R}_0 < 1$, whereas a unique endemic equilibrium exists whenever $\mathscr{R}_0 > 1$. Local asymptotic stability of the endemic equilibrium is conditional on the associated Routh–Hurwitz criteria and is verified numerically for the baseline parameter set through direct computation of the Jacobian eigenvalues. Furthermore, the bifurcation analysis established the existence of a forward transcritical bifurcation at the critical threshold $\mathscr{R}_0 = 1$. The analytical findings were supported by numerical simulations, which illustrated the qualitative behaviour of the system under different epidemiological scenarios. Sensitivity analysis identified the effective transmission rate as the most influential parameter governing HIV persistence, while the parameters associated with treatment failure and resistance progression were also found to contribute substantially to sustained disease transmission. These findings underscore the epidemiological importance of reducing treatment failure and limiting progression toward drug-resistant infection classes.

An optimal control framework incorporating prevention measures, ART uptake, and adherence-support interventions was formulated and analysed using Pontryagin's Maximum Principle. For the state and control weights specified in **Table 3**, the combined three-control strategy reduced the cumulative infectious burden relative to the uncontrolled case over the simulated intervention horizon. The resulting control profiles also indicate an important role for sustained adherence support under the particular objective functional considered here. Because the present simulations do not provide a complete head-to-head comparison of every individual control with every combined strategy, no general ranking of individual versus integrated interventions is claimed. A systematic comparison of alternative control combinations, together with formal economic cost-effectiveness analysis under different weighting schemes, is left for future investigation. Although the proposed model captures several important epidemiological mechanisms, it does not explicitly incorporate transmitted drug resistance, heterogeneous adherence behaviour, treatment re-initiation, or viral re-suppression following salvage therapy. Future extensions may incorporate these mechanisms together with stochastic effects, population heterogeneity, and data-driven parameter estimation.

Author contributions: All authors contributed equally to the conceptualization, methodology, mathematical analysis, interpretation of the results, manuscript preparation, and critical revision of the work. All authors have read and approved the final version of the manuscript.

Funding: This research received no external research funding. The Article Processing Charge (APC) was supported by Prince Sultan University.

Institutional review board statement: Not applicable. This study is a theoretical mathematical modelling investigation and does not involve human participants, animals, or identifiable individual-level data.

Informed consent statement: Not applicable.

Data availability statement: No new datasets were generated or analysed in this study. All parameter values used in the numerical experiments are reported in the manuscript and were obtained from the cited literature.

Acknowledgment: The authors would like to acknowledge the support of Prince Sultan University for paying the Article Processing Charges (APC) of this publication.

Conflict of interest: The authors declare no conflicts of interest.

AI use statement: During the revision of this manuscript, ChatGPT, developed by OpenAI, was used to assist with language editing and the checking of clarity and consistency. All mathematical derivations, numerical computations, interpretations, and scientific conclusions were independently reviewed and verified by the authors. The authors take full responsibility for the content of the manuscript.

References

1. UNAIDS. Global HIV & AIDS Statistics - Fact Sheet 2025. UNAIDS; 2025. Available online: https://www.unaids.org/en/resources/fact-sheet
2. World Health Organization. HIV Data and Statistics. World Health Organization; 2025. Available online: https://www.who.int/teams/global-hiv-hepatitis-and-stis-programmes/hiv/strategic-information/hiv-data-and-statistics
3. Granich R, Gupta S, Suthar AB, et al. Antiretroviral Therapy in Prevention of HIV and TB: Update on Current Research Efforts. Current HIV Research. 2011; 9(6): 446–469.
4. Naik PA, Yavuz M, Zu J. The role of prostitution on HIV transmission with memory: A modeling approach. Alexandria Engineering Journal. 2020; 59(4): 2513–2531.
5. Nowak MA, May RM. Virus Dynamics: Mathematical Principles of Immunology and Virology. Oxford University Press; 2000.
6. Kirschner D, Webb GF. A model for treatment strategy in the chemotherapy of AIDS. Bulletin of Mathematical Biology. 1996; 58(2): 367–390.
7. Blower SM, Aschenbach AN, Gershengorn HB, et al. Predicting the unpredictable: Transmission of drug-resistant HIV. Nature Medicine. 2001; 7(9): 1016–1020.
8. Perelson AS, Nelson PW. Mathematical Analysis of HIV-1 Dynamics in Vivo. SIAM Review. 1999; 41(1): 3–44.
9. Anderson RM, May RM. Infectious Diseases of Humans: Dynamics and Control. Oxford University Press; 1991.
10. Hethcote HW. The Mathematics of Infectious Diseases. SIAM Review. 2000; 42(4): 599–653.
11. Jan R, Boulaaras S, Khan IA, et al. Nonlocal and nonsingular kernel-based fractional dynamics of infectious disease with waning immunity. Journal of Mathematics and Computer Science. 2024; 38(1): 98–110.
12. Kongson J, Thaiprayoon C, Neamvonk A, et al. Investigation of fractal-fractional HIV infection by evaluating the drug therapy effect in the Atangana–Baleanu sense. Mathematical Biosciences and Engineering. 2022; 19(11): 10762–10808. doi: 10.3934/mbe.2022504
13. Khan H, Gómez-Aguilar JF, Alkhazzan A, et al. A fractional order HIV-TB coinfection model with nonsingular Mittag-Leffler Law. Mathematical Methods in the Applied Sciences. 2020; 43(6): 3786–3806. doi: 10.1002/mma.6155
14. Haq IU, Ali A, Ullah A, et al. Mathematical analysis of fractional order co-abuse infection model using power law type kernel. Journal of Mathematics and Computer Science. 2025; 36: 352–370. doi: 10.22436/jmcs.036.04.01
15. Naeem M, Kuang Y, Li J. Stability of linear delay differential systems via Laplace transformation. Mathematical Biosciences. 2026; 400: 109778. doi: 10.1016/j.mbs.2026.109778
16. Liu X, Wang H, Hu Z, et al. Global stability of an HIV pathogenesis model with cure rate. Nonlinear Analysis: Real World Applications. 2011; 12(6): 2947–2961. doi: 10.1016/j.nonrwa.2011.04.016
17. Huo HF, Feng LX. Global stability for an HIV/AIDS epidemic model with different latent stages and treatment. Applied Mathematical Modelling. 2013; 37(3): 1480–1489. doi: 10.1016/j.apm.2012.04.013
18. Xue L, Sun Y, Ren X, et al. Modelling the transmission dynamics and optimal control strategies for HIV infection in China. Journal of Biological Dynamics. 2023; 17(1): 2174275.
19. Abimbade SF, Chuma FM, Olaniyi S, et al. Lyapunov Stability and Optimization of a Fractional-Order HIV/AIDS Model Coupling Vertical Transmission With Saturated Treatment. International Journal of Mathematics and Mathematical Sciences. 2026; 2026(1): 3059683.
20. Kumar N, Kashif M, Chauhan TS, et al. Modeling and Control of HIV/AIDS Epidemics: A Stochastic and Optimal Control Perspective. Journal of Nonlinear Mathematical Physics. 2025; 32(1): 80.
21. Elmojtaba IM. An optimal control analysis of HIV-Visceral Leishmaniasis co-infection model. Partial Differential Equations in Applied Mathematics. 2025; 14: 101216.
22. Ahmad I, Ahmad I, Ali N. Impact of Awareness and Protective Measures on the Transmission Dynamics of HIV/AIDS: A Mathematical Analysis. International Journal of Applied and Computational Mathematics. 2025; 11(3): 102.
23. Diekmann O, Heesterbeek JAP, Roberts MG. The construction of next-generation matrices for compartmental epidemic models. Journal of The Royal Society Interface. 2010; 7(47): 873–885.
24. Van Den Driessche P, Watmough J. Reproduction numbers and sub-threshold endemic equilibria for compartmental

models of disease transmission. Mathematical Biosciences. 2002; 180(1–2): 29–48.
25. Castillo-Chavez C, Song B. Dynamical Models of Tuberculosis and Their Applications. Mathematical Biosciences and Engineering. 2004; 1(2): 361–404.
26. Castillo-Chavez C, Feng Z, Huang W. On the computation of $\mathscr{R}_0$ and its role on global stability. In: Mathematical Approaches for Emerging and Reemerging Infectious Diseases: An Introduction. Springer; 2002. pp. 229–250.
27. Omame A, Isah ME, Abbas M, et al. A fractional order model for Dual Variants of COVID-19 and HIV co-infection via Atangana-Baleanu derivative. Alexandria Engineering Journal. 2022; 61(12): 9715–9731.
28. Teklu SW, Guya TT, Kotola BS, et al. Analyses of an age structure HIV/AIDS compartmental model with optimal control theory. Scientific Reports. 2025; 15(1): 5491.
29. Chitnis N, Hyman JM, Cushing JM. Determining Important Parameters in the Spread of Malaria Through the Sensitivity Analysis of a Mathematical Model. Bulletin of Mathematical Biology. 2008; 70(5): 1272–1296.
30. Pontryagin LS, Boltyanskii VG, Gamkrelidze RV, et al. The Mathematical Theory of Optimal Processes. Wiley; 1962.
31. Lenhart S, Workman JT. Optimal Control Applied to Biological Models. CRC Press; 2007.
32. Hussein AA, Mebrate B. A Fractional Order Model for HIV/AIDS With Treatment and Optimal Control Using Caputo Derivative. International Journal of Mathematics and Mathematical Sciences. 2025; 2025(1): 9342227. doi: 10.1155/ijmm/9342227
33. Peter OJ, Teklu SW, Balogun GB, et al. HIV/AIDS compartmental model analysis with drug resistance treatment, vertical transmission, and optimal control theory. Scientific Reports. 2025; 15(1): 44156.
34. Marsudi M, Trisilowati T, Musafir RR. Bifurcation and Optimal Control Analysis of an HIV/AIDS Model with Saturated Incidence Rate. Mathematics. 2025; 13(13): 2149.
35. Poonia A, Chakrabarty SP. Strategic Control of Drug-Resistant HIV: Multi-Strain Modeling with Diagnosis, Adherence, and Treatment Switching. Bulletin of Mathematical Biology. 2025; 87(12): 173.
36. Brauer F. Compartmental models in epidemiology. In: Mathematical Epidemiology. Springer; 2008. pp. 19–79.
37. Perko L. Differential Equations and Dynamical Systems, 3rd ed. Springer; 2001. doi: 10.1007/978-1-4613-0003-8
38. Khalil HK. Nonlinear Systems, 3rd ed. Prentice Hall; 2002. ISBN: 978-0-13-067389-3.
39. Shuai Z, Van Den Driessche P. Global Stability of Infectious Disease Models Using Lyapunov Functions. SIAM Journal on Applied Mathematics. 2013; 73(4): 1513–1532.
40. Fleming WH, Rishel RW. Deterministic and Stochastic Optimal Control. Springer-Verlag; 1975.